eLife Title: A calcineurin-mediated scaling mechanism that controls a K^+-leak channel to regulate morphogen and growth factor transcription

Chao Yi[1,2], Tim WGM Spitters[1*], Ezz Al-Din Ahmed Al-Far[3*], Sen Wang[1,2], Tian Long Xiong[1,2], Simian Cai[1], Xin Yan[1], Kaomei Guan[3], Michael Wagner[3,4], Ali El-Armouche[3] and Christopher L. Antos[1,3]†

[1]School of Life Sciences and Technology, ShanghaiTech University, 230 Haike Road, Shanghai, People's Republic of China.

[2] CAS Center for Excellence in Molecular Cell Science, Shanghai Institute of Biochemistry and Cell Biology, Chinese Academy of Sciences, University of Chinese Academy of Sciences

[3]Institut für Pharmakologie und Toxikologie, Technische Universität Dresden, Fetscherstraße 74, 01307 Dresden, Germany

[4] Klinik für Innere Medizin und Kardiologie, Herzzentrum Dresden, Technische Universität Dresden, Fetscherstraße 76, 01307 Dresden, Germany

*These two authors contributed equally.

Running Title: Kcnk5b coordination of developmental transcription

Key words: regeneration, development, zebrafish appendages, proportional growth, membrane potential, morphogens

†Corresponding Author:
Christopher L. Antos
School of Life Sciences and Technology
ShanghaiTech University,
230 Haike Road
Pudong, New District,
Shanghai, China 201210
clantos@shanghaitech.edu.cn

Abstract

The increase in activity of the two-pore potassium-leak channel Kcnk5b maintains allometric juvenile growth of adult zebrafish appendages. However, it remains unknown how this channel maintains allometric growth and how its bioelectric activity is regulated to scale these anatomical structures. We show the activation of Kcnk5b is sufficient to activate several genes that are part of important development programs. We provide *in vivo* transplantation evidence that the activation of gene transcription is cell autonomous. We also show that Kcnk5b will induce the expression of different subsets of the tested developmental genes in different cultured mammalian cell lines, which may explain how one electrophysiological stimulus can coordinately regulate the allometric growth of diverse populations of cells in the fin that use different developmental signals. We also provide evidence that the post-translational modification of serine 345 in Kcnk5b by calcineurin regulates channel activity to scale the fin. Thus, we show how an endogenous bioelectric mechanism can be regulated to promote coordinated developmental signaling to generate and scale a vertebrate appendage.

Introduction

Tissue scaling involves the coordinated control of developmental programs, since anatomical structures consist of different tissues that form in a coordinated manner and grow proportionally with each other and with the body. While there are several developmental signals known to regulate cell proliferation and tissue formation, mechanisms that concomitantly activate several developmental signals to synchronize the growth of multi-tissue appendages and organs in a manner that is coordinated with body proportions remain poorly defined.

There is growing evidence that several biological phenomena involved in tissue generation and growth are influenced by electrophysiological changes in "non-excitable" cells (Sundelacruz et al., 2009). Several cell behaviors are affected by the addition of electric currents (McCaig et al., 2005): cell migration, cell proliferation, cell differentiation, gene transcription and consequently tissue formation are all altered by the application of an exogenous current (Baer and Colello, 2016; Bartel et al., 1989; Blackiston et al., 2009; Borgens et al., 1977; Geremia et al., 2007; Sundelacruz et al., 2009; Yasuda, 1974; Zhao et al., 2002). The culmination of these findings have led to the hypothesis that bioelectrical fields exist that have higher order organizational non-cell-autonomous properties in the development of anatomical structures [For review, see (Levin, 2014; Messerli and Graham, 2011)].

As a regulator of membrane potential, K^+ conductance is an important component of the electrophysiological properties of cells. Evidence that illustrates the importance of K^+ conductance in tissue formation comes from studies in which disruption of inward rectifying K^+ channels of the Kir2 family can cause cranial facial defects, abnormal number of digits and reduced digit size (Andersen et al., 1971; Canun et al., 1999; Sansone et al., 1997; Tawil et al., 1994; Yoon et al., 2006a; Yoon et al., 2006b; Zaritsky et al., 2000). A striking finding concerning the coordinated control of cell behavior is the formation of eye structures by overexpressing different ion channels that alter membrane potential in early *Xenopus* embryos (Pai et al., 2012): overexpression and activation of a glycine-gated chloride channel in cells that form the eye interferes with eye formation, while overexpression of a dominant-negative K^+-ATP channel simulates ectopic eye formation even in unexpected locations on the body (Pai et al., 2012). These findings illustrate that changes in the membrane potential of cells can have significant impacts on the development of anatomical structures. However, how electrophysiological information associates with the multiple necessary signals that control formation and/or growth of multi-tissue structures remains unclear.

The development of body structures not only involves forming tissues, it also involves coordinating the growth of each contributing tissue cell. To form organs that correctly scale with the body, each tissue grows either isometrically (grows with the same rate as the body) or allometrically (disproportionally grows in relation to the growth of the body). The zebrafish mutants *another long fin* (*alf*), *long fin* (*lof*) and *schleier* (*schl*) display continued allometric growth of each appendage from the juvenile stage into the adult stage (Lanni et al., 2019; Perathoner et al., 2014; Stewart et al., 2020). The dominant allometric growth phenotype of *alf* is due to mutations in the transmembrane pore region of *kcnk5b* (Perathoner et al., 2014), encoding a two-pore K^+-leak channel that regulates membrane potential by outward flow of K^+ from the cell (Goldstein et al., 2001). The dominant phenotype of *lof* is linked to elevated expression of a voltage-gated potassium channel *Kcnh2a* (Stewart et al., 2020). The phenotype of *schl* is due to dominant-negative mutations in *scc4* (Lanni et al., 2019), encoding a K^+-Cl^- cotransporter that regulates intracellular K^+ levels in a chloride-dependent manner (Marcoux et al., 2017). *alf*, *lof* and *schl* demonstrate the importance of K^+ conductance and ultimately of electrophysiological signals for the correct body-to-appendage proportions. Despite the connection between K^+ conductance and the proportional growth of the fins, it remains unclear how K^+-mediated signal translates into coordinated growth of the fish appendage and how any K^+ channel is regulated to scale tissue.

We show that activity of the single two-pore K^+-leak channel Kcnk5b is sufficient to induce the activation of at least two components, Shh and Lef1, of two important morphogen pathways, not only in the adult fin but also in the larva. Our data also indicates that this induction is cell autonomous, arguing that increases in membrane potential caused by Kcnk5b regulate growth through intracellular regulation of these developmental pathways. Overexpression of *kcnk5b* or one of two other two-pore *kcnk* channels in different mammalian cell lines showed variable activation of genes belonging to different developmental signal transduction mechanisms, supporting the conclusions that the different developmental mechanisms needed to scale fish appendages can be regulated by the same electrophysiological change induced by potassium leak and that the combinatorial activation of the different developmental mechanisms by Kcnk5b is cell-type dependent. Lastly, we provide evidence for how post-translational modification of Kcnk5b at Serine345 by calcineurin regulates its electrophysiological activity and consequently the scaling of zebrafish fins. Thus, we describe an endogenous cell-autonomous mechanism through which electrophysiological signals can induce and coordinate specific morphogen and growth factor signals to mediate the scaling of an anatomical structure.

Results

Kcnk5b is sufficient to induce several developmental gene programs in different cell types in adult and larva.

Mutations in the two-pore K^+-leak channel Kcnk5b that increase its activity lead to enhanced growth of the zebrafish appendages (Perathoner et al., 2014). While this finding implicates the importance of bioelectric signaling in appendage scaling, it remains unknown how the activity of a single K^+ channel is integrated with the developmental controls that generate new appendage tissues. Growth of any appendage involves the coordinated activation of specific morphogen and growth factor pathways: Shh, β-catenin-dependent Wnt, Bmp, Fgf and Retinoic acid. Therefore, to begin to determine how this channel is involved in the coordinated growth of the entire fin, we generated transgenic zebrafish that expresses *kcnk5b* under the control of a conditionally inducible promoter (heat-shock promoter) to temporally activate this channel in adult fins. After a single ten-minute heat-shock pulse of the Tg[*hsp70*:*kcnk5b*-GFP] transgene, we observed significant activation of *shh* and *lef1* (β-catenin-dependent Wnt) (Fig. 1Aa; Fig.1-Suppl. Fig. 1A), as well as an increase in *aldh1a2* (retinoic acid) (Fig. 1Ab) within 6 hours by qRT-PCR, while *pea3* (Fgf) was slightly increased and *msxb* (BMP) was not significantly changed (Fig. 1A). All genes returned to control levels by 12 hours after the single pulse (Fig. 1B). The induction of the developmental genes coincided with the temporal expression of the *kcnk5b*-GFP transgene (Fig. 1C), whose expression emerged as a lattice pattern(Fig. 1-Suppl. Fig. 1B-D), indicating that Kcnk5b-GFP was localized and functioned at cell membranes. When we maintained chronic expression of the transgene by heat shocking the caudal fin for 10 minutes once per day for 3 days, we observed expression of *lef1*, *shh*, *aldh1a2* as well as *pea3* and *msxb* over controls (Fig. 1D), which included Shh's patched receptors and slight up-regulation of *bmp2b* (Fig. 1-Suppl. Fig. 1E). Together, these data show that Kcnk5b is sufficient to induce the transcription of certain developmental genes as though it were a part of their signaling mechanisms. Furthermore, the initial activation of *shh*, *lef1* and *aldh2a* (Fig. 1A) followed by later upregulation of *pea3* and *msxb* after continued *kcnk5b* overexpression (Fig. 1C) suggest that there is a hierarchical activation of developmental mechanisms that will ultimately lead to the complete allometric growth program.

To examine the spatial expression of the two genes most responsive to Kcnk5b, we performed *in situ* hybridization experiments for *shh* and *lef1*. Compared to control fins (Fig. 3Ea,c) , localization of *shh* and *lef1* was in the distal tip of the fin (Fig. 1Eb,d) where growth normally occurs, and cross sections through the fins showed that Kcnk5b-mediated induction

of these genes occured in the epidermal/epithelial tissues (Fig. 1Fb,d). We also assessed increases in Shh and Lef1 protein levels after the heat-shock induction of *kcnk5b*-GFP (Fig. 1G,H; Fig. 1-Suppl. Fig. 2A,B). Because Lef1 conveys β-catenin-dependent Wnt signaling by acting as a transcriptional platform for β-catenin, we examined protein expression of β-catenin and observed no significant differences in its overall levels (Fig. 1G,H; Fig. 1-Suppl. Fig. 2C). However, when we examined β-catenin protein distribution in the fin tissues by immunohistochemistry staining, we observed an increased number of nuclei with β-catenin co-staining in the outer epidermis layers and basal epithelium of the fin (Fig. 1I,J; Fig. 1-Suppl. Fig. 2E-J) despite no significant differences in the measured β-catenin-associated fluorescence intensities (Fig. 1-Suppl. Fig. 2K). To test whether the redistribution of β-catenin leads to the activation of known β-catenin-dependent genes, we performed qRT-PCR of *axin2*, *cyclin D* and *c-myc*. We observed that none of these candidates were activated (Fig. 1K), which indicates that while Lef1 expression increases, β-catenin-dependent Wnt signaling is not directly activated by Kcnk5b. Together, all the expression results indicate that Kcnk5b activity promotes the transcription of specific components of a limited number of developmental pathways in the adult fint.

To test whether increasing the activity of Kcnk5b has the same transcriptional effect on these developmental pathways in another *in vivo* context, we induced the expression of *kcnk5b* in the zebrafish larva (Fig. 2-Suppl. Fig. 1A). We observed that *lef1, shh, adlh2a, pea3 and msxb* expression levels were increased by induction of *kcnk5b* compared to heat-shocked non-transgenic control fish (Fig. 2A). To further explore the effect of Kcnk5b activity on *shh* transcription in developing fins, we performed *in situ* hybridization experiments on fish embryos and examined *shh* expression in the developing pectoral fin buds. Compared to the emerging expression of *shh* in the fin buds of heat-shocked non-transgenic embryos (Fig. 2Ba,c), we observed *kcnk5b* expression induced increases in the rate of *shh* mRNA detection (Fig. 2Bb,d) and in the area of *shh* expression (Fig. 2Be-h). Thus, Kcnk5b activity appears to increase both the intensity (Fig. 2Bi) and the range of *shh* expression (Fig. 2Bj). We further assessed Lef-1-dependent transcription by crossing the heat-shock-inducible transgenic Tg[*hsp70*:*knck5b*-GFP] line with the transgenic Lef1 reporter line Tg[*7XTCF-Xla.sam:*mCherry]. While the double-transgenic fish Tg[*hsp70*:*kcnk5b*-GFP; *7XTCF-Xla.sam:*mCherry] displayed limited expression of mCherry before heat-shock induction of the *kcnk5b*-GFP transgene (Fig. 2Ca,b,g), after heat shock, double-transgenic Tg[*hsp70*:*kcnk5b*-GFP; *7XTCF-Xla.sam:*mCherry] fish showed a broad increase in reporter mCherry expression over single-transgenic Tg[*7XTCF-Xla.sam:*mCherry] (Fig. 2Cd,e,g). From histological cross

sections of double-transgenic larva, we observed that mCherry was upregulated broadly in the body of the animal (Fig. 2D). Furthermore, we observed an increase in the length of the caudal finfold along the anterioposterior axis of 5 dpf larva after induction of *kcnk5b*-GFP by single daily 10-minute pulses over 3 days (Fig. 2F; Fig. 2-Suppl. Fig. 1C), while the caudal finfold lengths along the dorsoventral axis of appeared not change (Fig. 2G). However, we observed that when we compared both anterioposterior and dorsoventral axes measurements in relation to body length, we observed that in both instances the finfold dimensions proportionally increased (Fig. 2H,I), which was in part associated with decreases in the lengths of the bodies (Fig. 2J). These results showed that in relation to the body, Kcnk5b activity promoted proportional increases in the finfold dimensions. Our observation that the activity of this channel decreased the length of the body, suggests that the growth-promoting effects of Kcnk5b activity may be limited to the finfolds and appendages. Together, these results indicate that Kcnk5b activity is sufficient to promote the transcription of specific developmental genes in several different tissue types to promote allometric growth of the finfold.

Activation of the Lef1-dependent transcription by Kcnk5b is cell autonomous in several different tissues

Previous work implicates bioelectric intercellular communication as a mechanism for how bioelectricity can influence tissue growth (McLaughlin and Levin, 2018), and changes in K^+ channel activity have been shown to regulate different cell behaviors in a non-cell-autonomous manner (Morokuma et al., 2008; Pai et al., 2015). The broad activation of the Lef1-dependent Wnt reporter in several tissues (Fig. 2) and Kcnk5b's ability to scale all the tissues of the fin appendages suggest that Kcnk5b acts via non-cell autonomous communication among cells. To determine whether the observed Kcnk5b-mediated induction of gene expression is due to intercellular communication (e.g., through extracellular ligands such as Wnt) or due to cell autonomous activation of transcription, we transplanted cells from Tg[*hsp70*:*kcnk5b*-GFP; *7XTCF-Xla.sam*:mCherry] transgenic embryos into embryos harboring only the Tg[*7XTCF-Xla.sam*:mCherry] transgene and then raised mosaic embryos and larva (Fig. 3A). Analyses of the mosaic larva showed the previously reported developmental expression of the Lef1-dependent reporter before heat shock (Fig. 3Ba,e,i,m)(Moro et al., 2012). However, after heat-shock induction of the Tg[*hsp70*:*kcnk5b*-GFP] transgene (Fig. 3Bb,f,j,n), we observed ectopic activation of *7XTCF-Xla.sam*:mCherry reporter only in donor cells of chimeric 48 hpf and 72 hpf fish (recipient *7XTCF-Xla.sam*:mCherry fish harboring transplanted cells from Tg[*hsp70*:*kcnk5b*-GFP;*7XTCF-Xla.sam*:mCherry] embryos). GFP-mCherry-positive cells

appeared in tissues in the head (Fig. 3Bb,c,d), in skeleton surrounding the eye (Fig. 3Bf,g,h), in trunk muscles (Fig. 3Bj,k,l) and in skin (Fig. 3Bn,o,p). From closer inspection, we observed co-expression in neurons in the head (Fig. 3Ca-c), in the ectodermal bones of the skull (Fig. 3Cd-f), mandible bone and cartilage (Fig. 3Cg-i), mesenchyme surrounding the otic vesicle (Fig. 3Cj-l), epithelial cells in the finfold (Fig 3Co-r) and individual striated muscle cells of the trunk (Fig. 3Cr-t). We counted the number of GFP and mCherry positive cells in the different tissues and observed that all Kcnk5b-GFP-positive cells were mCherry positive (Fig. 3C). Moreover, in all tissues, the ectopic mCherry expression was always limited to the Kcnk5b-positive cells (Fig. 3B- E; Fig. 3-Suppl. Fig. 1G-J). Together, these data support two conclusions: one, the activation of the Lef1-dependent reporter by Kcnk5b is cell autonomous; and two, Kcnk5b is able to promote the expression of the Lef1 reporter in diverse tissue types.

As a K^+-leak channel, Kcnk5b's activity should decrease intracellular K^+ levels. We performed Fluorescence Lifetime Microscopy (FLIM) analysis with an established genetic sensor for K^+ to measure intracellular K^+ levels (Shen et al., 2019). This sensor uses the FRET potential between two fluorophores that are joined by a K^+-binding linker. Changes in FRET due to K^+ binding results in changes in the fluorescence lifetime of the fluorophores, which allows for the assessment of intracellular K^+ levels. Transfection of the channel in Human Embryonic Kidney HEK293T cells (Fig. 4-Suppl. Fig. 1A-L) resulted in significant increase in CFP fluorescence lifetime due to decreased FRET of the sensor compared to control transfected cells (Fig. 4Aa-c,g), which indicated reduced intracellular K^+ levels in the cells that express Kcnk5b (Fig. 4Ad-g). Additional higher resolution assessments along the lateral borders of cells showed similar increases in CFP fluorescence lifetime along the plasma membrane, indicating expected reduction of K^+ levels at the cell membrane by active Kcnk5b (Fig. 4-Suppl. Fig. 1M-O).

To test whether activity *kcnk5b* promotes the gene expression profile in mammalian cells that we observed in the zebrafish, we expressed *kcnk5b* either by establishing stable HEK293T (HEK) cells lines that either express GFP or zebrafish *kcnk5b*-GFP or by transient transfections. From qRT-PCR analyses comparing HEK cells expressing either GFP or *kcnk5b*-GFP, we observed an increase in SHH and PEA3 expression (Fig. 4Ba; Fig. 4-Suppl. Fig. 2A) and the down-regulation of LEF1, ALDH1a2 and MSX1 (Fig. 4Bb; Fig. 4-Suppl. Fig. 2B). To determine whether this transcriptional response is specific to Kcnk5b or is a general response to two-pore K^+-leak channels, we transfected cells with one of two K^+-leak channels Kcnk9 and Kcnk10 (Fig. 4-Suppl. Fig 2C,D). Transfection of HEK cells with these two other channels

resulted in a similar HEK-cell transcriptional profile as Kcnk5b for SHH and FGF (Fig. 4C), indicating that this transcriptional response to Kcnk5b is a response to the electrophysiological changes associated with intracellular K^+ leak.

The differences between the transcriptional responses of the zebrafish adult, larva and HEK cells indicate that different cell types will have different responses to Kcnk5b electrophysiological activity. Therefore, we examined the transcriptional responses to Kcnk5b in other mammalian cell lines. In HeLa cells, Kcnk5b induced PEA3 and LEF (Fig. 4D). In the N2A (neural carcinoma) cell line, we observed the increase of ALDH1a2 (Fig. 4E) but decreases in SHH, LEF1 and PEA3 (Fig. 4F). In the MYF7 epithelial carcinoma cell line, Kcnk5b induced ALDH1a2, PEA3 and MSX1 (Fig. 4G).

When we tested whether Kcnk9 and Kcnk10 produce similar transcription profiles as Kcnk5b in HELA and N2A cells, we observed similar profiles between Kcnk9 and Kcnk10 (Fig. 4H-L), but differences between their outcomes and the transcriptional outcome of Kcnk5b. In HELA cells, the transcriptional response of PEA3 and ALDH2A to Kcnk9 and -10 were different than that of Kcnk5b (Fig. 4D,I-J). In N2A cells, while we observed similar increases in Aldh2A transcription and similar trends for Pea3 (Fig. 4E,F,K,L), we also observed the lack of down regulation of Shh, Lef1 and Pea3 (Fig. 4E,F,K,L). Together, these results reveal that Kcnk channel activity is sufficient to induce the transcription of genes associated with different developmental pathways in different mammalian cells types, and indicate that the downstream consequences of membrane potential changes are not intrinsic to specific signal transduction pathways. We propose that the variability in gene transcription in different cell types may explain why the solitary change in the activity of this channel in all cells of the fin leads to the variable transcriptional responses that promote coordinated growth of a multi-tissue anatomical structure.

Calcineurin regulates Kcnk5b channel activity and Kcnk5b-mediated gene transcription

We previously showed that the phosphatase calcineurin acts as a molecular switch between isometric and allometric proportional growth of the zebrafish fins (Kujawski et al., 2014). The similarities in the phenotypes produced by calcineurin inhibition and by the mutations in Knck5b that enhance Kcnk5b channel activity suggest a direct functional relationship between them (Kujawski et al., 2014; Perathoner et al., 2014). Based on whole-cell patch-clamp experiments, the mutations in *kcnk5b* that maintain allometric growth of the fins

also increased K^+ conductance at the plasma membrane (Perathoner et al., 2014). Therefore, we hypothesized that calcineurin inhibition will increase *in vivo* K^+ conductance and promote allometric growth of the zebrafish fins (Fig. 5A). To test whether calcineurin alters the channel activity of Kcnk5b, we examined the activity of Kcnk5b in the presence of calcineurin. Comparison of whole-cell patch-clamp measurements using HEK cells showed that Kcnk5b expression increases current density due to K^+ leak from the cells (Fig. 5B), as we observed from FRET-FLIM intracellular K^+ measurements (Fig. 4A). However, cells co-expressing both *knck5b* and calcineurin decreased the K^+ conductance of the cells compared to cells expressing *kcnk5b* alone (Fig. 5B). We then tested whether inhibition of the endogenous calcineurin activity in the HEK cells by the calcineurin inhibitor FK506 affects Kcnk5b channel activity. We found that FK506 treatment of cells expressing *kcnk5b* resulted in a significant increase in K^+ current compared with DMSO-treated *kcnk5b*-expressing cells (Fig. 5C). These results show that changes in calcineurin activity alter Kcnk5b channel activity in a manner that is constant with the enhanced fin growth induced by calcineurin inhibition and the increased channel activity of the *kcnk5b* zebrafish mutants, which indicates a functional interaction between calcineurin and Kcnk5b.

Calcineurin interacts with its substrates at particular amino acid sequence sites (Grigoriu et al., 2013). Our analysis of the amino acid sequence in the C-terminal cytoplasmic tail of Kcnk5b suggests a functional calcineurin binding site (LVIP) is present (Fig. 5A, red letters). To test for functional interaction at this site, we mutated the amino acid sequence (Fig. 5D, red letters) and assessed how the mutation affected the ability of calcineurin to regulate the channel. Compared to the decrease in activity of the wild-type channel after co-transfection with calcineurin, co-transfection of the Kcnk5b mutant lacking the calcineurin binding site (Kcnk5bmut+CaN) showed that the mutation made the channel resistant to calcineurin-mediated inhibition (Fig. 5D). The resistance of the Kcnk5bmut to calcineurin indicated that the repression of channel activity on Kcnk5b by calcineurin is due to the interaction of these to proteins at the LVIP site.

The regulation of Kcnk5b by calcineurin suggests that changes in calcineurin activity will have an effect on the Kcnk5b-dependent gene expression. To assess whether the activation of SHH by Knck5b can be altered by calcineurin, we compared the expression of SHH between HEK cells stably expressing GFP and HEK cells stably expressing the Kcnk5b channel as well as between HEK cells stably expressing the channel after transfection with calcineurin. We observed that compared to channel expression alone, co-expression of calcineurin decreased the Kcnk5b-mediated induction of SHH (Fig. 5E) and PEA3 (Fig. 5F). To determine whether

calcineurin effect on Kcnk5b-medidated SHH expression is specific to Kcnk5b, we transfected HEK cells with Kcnk9 or Kcnk10. Both Kcnk9 and Kcnk10 lack identifiable calcineurin binding sites (Fig. 4-Suppl. Fig. 2C,D), and we observed that unlike the effect on Kcnk5b, calcineurin had no effect on the induction of SHH (Fig. 5G) or PEA3 (Fig. 5H) by Kcnk9 or by Kcnk10, indicating that calcineurin's regulation of the electrophysiological induction of SHH and PEA3 transcription is specific to Kcnk5b.

Calcineurin regulates Kcnk5b through S345 to scale the fin

As a phosphatase, calcineurin should regulate Kcnk5b by dephosphorylating the channel at specific serine or threonine residues. A specific serine in the C-terminal tail represented a typical consensus serine-proline (Ser345-Pro346) phosphorylation site for calcineurin (Fig. 6A). Therefore, we hypothesized that calcineurin inhibits the activity the Kcnk5b channel by dephosphorylating this serine. We tested whether rendering the Kcnk5b channel unphosphorylatable at this serine by alanine substitution (S345A) would decrease the channel's activity. Whole-cell patch-clamp experiments of the *kcnk5bS345A* showed a significant decrease in K^+ conductance of the channel compared to the wild-type (*kcnk5bS345*) control (Fig. 6B). To assess the specificity of the reduction effect for this serine, we also systematically substituted adjacent serines with alanines and subsequently measured channel activity (Fig. 6-Suppl. Fig. 1A). While *kcnk5bS345A* showed reduction in activity, the substitution of other serines did not (Fig. 6C, Fig. 6-Suppl. Fig. 1A-D).

To determine whether the activity of the Kcnk5b channel is associated with the phosphorylation state of this serine, we exchanged the serine for a glutamic acid in order to mimic serine phosphorylation (*kcnk5bS345E*) (Fig. 6C). Expression of this mutant displayed elevated K^+ conductance compared to *knck5bS345* wildtype channel (Fig. 6D). In addition, the *kcnk5bS345E* mutant was resistant to calcineurin-mediated inhibition (Fig. 6D). Moreover, the substitution of other serines with glutamic acid had no effect on channel activity, and calcineurin could still regulated the channel (Fig. 6-Suppl. Fig. 1A,E,F). Together, these results indicate that S345 is the important post-translational regulatory serine involved in calcineurin-mediated regulation of Kcnk5b activity.

To determine whether there is a functional relationship between fin scaling and S345-mediated Kcnk5b channel activity, we placed the cDNA of each channel version (wild-type *kcnk5bS345*, *kcnk5bS345E* or *kcnk5bS345A*) under the control of the heat-shock inducible *hsp70* promoter to generate conditionally inducible transgenes for *in vivo* expression in the fish. We heat shocked the caudal fins of non-transgenic and transgenic fish lines once daily and

subsequently measured the length of each fin in relation to the length of each body (fin-to-body ratio). Non-transgenic siblings were included in the same heat-shock regimen to serve as controls. After 12 days of the heat-shock regimen, we noticed differences between the rates of the regenerating caudal fins lobes of the different transgenic lines (Fig. 6E) after standardizing the length of each fin to the length of the body (Fig. 6-Suppl. Fig. 1G). By assessing regenerating lobe-to-body measurements over time, we observed that Tg[*hsp70*:*kcnk5bS345E*] fish maintained the highest rates of allometric regenerative growth, while Tg[*hsp70*:*kcnk5bS345A*] displayed the lowest growth rates of the transgenic lines (Fig. 6E). There was no significant change in the rates of growth of the bodies (Fig. 6-Suppl. Fig. 1G). We also assess the final proportional size of unamputated fin lobes between the different transgenic lines, and we observed a linear relationship between the proportional length of the unamputated lobes and the putative phosphorylation status of the channels: the S345A dephosphorylation mimic displayed the smallest growth proportions (Fig. 6I), the S345E phosphorylation mimic displayed the largest growth proportions (Fig. 6I), and the average value of the wild-type regulatable version of the channel was between the highly active S345E and marginally active S345A mutants (Fig. 6I).

To determine whether similar growth effects are generated by other two-pore K^+ leak channels, we generated a transgenic fish line that overexpresses *kcnk9*, Tg[*hsp70*:*kcnk9*-GFP]. Compared to transgenic fish that were not heat-shocked (Fig. 6Ja,K) and heat-shocked of non-transgenic fish (Fig. 6K), we observed that heat-shock-induced overexpression of *kcnk9* in the adult fins increased fin outgrowth (Fig. 6Jb,K; Fig. 6-Suppl. Fig. 1H), which further supports the conclusion that Kcnk5b-mediated growth is due to its regulation of its electrochemical properties.

Our ability to control the rate of growth by mimicking a specific post-translational modification that can be mediated by calcineurin and that correspondingly determines the level of Kcnk5b activity supports the conclusion that calcineurin regulation of Kcnk5b is an *in vivo* electrophysiological mechanism through which controlling the potassium conductance of cells scales a vertebrate appendage.

Discussion

Anatomical structures consist of a combination of different tissue types that develop and grow in a coordinated manner. Recent discoveries show that K^+ channels regulate the scaling of fish appendages, but it is still unclear how this electrophysiological signal controls several diverse developmental phenomena within this anatomical structure to achieve coordinated developmental growth. Our results reveal that this *in vivo* electrical signal has a hierarchical effect on specific developmental genes in the fish fins and larva.

Two-pore K^{+-}leak channels such as Kcnk5b allow K^+ to cross the membrane to establish an electrochemical equilibrium, this activity directly affects the membrane potential of the cell (Goldstein et al., 2001). Normally, the concentration of K^+ is higher on the cytoplasmic side of the plasma membrane due to continual active transport of K^+ into the cell by the ATP-dependent Na^+/K^+ pumps (Shattock et al., 2015). As a leak channel, opening of Kcnk5b causes a flow of K^+ out of the cell, which hyperpolarizes the membrane potential (Goldstein et al., 2001). The previous findings that mutations that increase Kcnk5b channel activity are associated with maintaining allometric growth (Perathoner et al., 2014) argue that such changes in membrane potential promote disproportional growth. Our current findings further these previous findings by showing that conditional induction of Kcnk channel activity is sufficient to induce morphogen pathways (Fig. 1,2,4) in different *in vivo* and *in vitro* contexts, demonstrating transcriptional control of particular developmental mechanisms by different two-pore K^+-leak channels.

In addition to K^+-leak channels, cells regulate intracellular K^+ through different channels and exchangers. Inward rectifying K^+ channels allow K^+ to enter the cell along the ion's electrochemical gradient. Exchangers will exchange K^+ with different substrates (e.g., Na^+) to facilitate the entry or removal of K^+ based on the concentration gradient of K^+ and the exchanged substrate. Previous findings show the importance of the inward rectifying K^+ channel Kir2 for cranial-facial and digit defects in humans (Andersen et al., 1971; Canun et al., 1999; Sansone et al., 1997; Tawil et al., 1994; Yoon et al., 2006a; Yoon et al., 2006b). Knockout of the mouse Kir2 channels results in similar head and digit defects (Zaritsky et al., 2000), and dominant-negative inhibition of the Drosophila Kir2 leads to wing appendage defects that are analogous to the human and mouse appendage defects (Dahal et al., 2012). While the mammalian phenotypes remain unexplained, the defects in the Drosophila wings have been linked to reduced Dpp (BMP) signaling (Dahal et al., 2012), suggesting that intracellular K^+ homeostasis is important for BMP signaling.

Removal of an ATP-sensitive K^+ channel in the early *Xenopus* embryo disrupts eye formation, while ectopic expression of this channel will produce ectopic eyes in the head and in locations that were not considered to be competent for producing eyes (Pai et al., 2012). The ability to ectopically generate eyes was linked to electrophysiological hyperpolarization of the cells and the activation of Pax6-eyeless gene (Pai et al., 2012), a master regulator for eye development (Chow et al., 1999; Halder et al., 1995). In planaria, shortly after wounding, membrane depolarization acts as an early anterior signal that is sufficient (even when induced on the posterior side) to promote the consequent formation of all the anterior structures of the planarian head by inducing notum expression, which inhibits β-catenin-dependent Wnt signal transduction (Durant et al., 2019). Furthermore, it was recently revealed that in the Drosophila wing discs, depolarization events promote membrane localization of the transmembrane receptor smoothened to promote Shh signaling and that membrane potential values are patterned within the wing disc (Emmons-Bell and Hariharan, 2021). These discoveries show that electrophysiological changes are important signals in the formation and growth of anatomical structures.

A recent finding showed that calcineurin inhibition or increased activity of the voltage-gated Kcnh2 channel (*lof* mutant) promotes regenerative outgrowth from the proximal side of a mid-fin excavation, a site that normally does not mount a regenerative outgrowth response (Cao et al., 2021). Our findings help explain how calcineurin-regulated and electrophysiological changes from potassium channels can lead to broader tissue organizing phenomena by showing the inductive effect that increasing K^+ conductance (and calcineurin's regulation of K^+ conductance) can have on a broad number of developmental pathways, which is important for coordinating the organized formation of tissues and organs. Furthermore, we posit that the effect of the activity of the Kcnk5b channel is broader than the traditional mechanisms of growth factor/morphogen signaling pathways, because it is not confined to specific signal transduction mechanisms; rather, it has variable broad effects, such as activation of several developmental signals in the adult fin (Fig. 1), the larva (Fig. 2) and different mammalian cell lines (Fig. 4). While we observed that Kcnk5b is sufficient to promote *lef1*-mediated transcription (Figs. 1-3), we did not observe direct activation of *axin2*, a down-stream target gene of β-catenin activity (Fig. 1-Suppl. Fig. 1C). We posit that Kcnk5b activity does not directly activate canonical Wnt, but primes cells for increased β-catenin activity upon the reception of a Wnt signal through up-regulation of Lef1. Ultimately, continued Kcnk5b activity must lead to increased β-catenin-dependent Wnt signaling, since all evidence indicates that Wnt signaling is required for allometric fin outgrowth (Kawakami et al., 2006; Stoick-Cooper et al.,

2007), and allometric fin growth is the phenotype that we get by *kcnk5b* or *kcnk9* overexpression in amputated and unamputated fins (Fig. 6E-L). We propose that the competence to activate different developmental pathways by electrophysiological changes is because the responding cells are either primed to activate them or the pathways are already active. It will be important to find out how this electrophysiological signal coordinates the activity of these developmental signals. In this regard, only few factors are known that regulate *shh* and *lef1* transcription. Thus, our finding that an electrophysiological mechanism is involved not only provides a new understanding of how electrophysiology acts as an inductive signal, it also may lead to the discovery of molecular mechanisms that control the expression of these mediators of important morphogen signals.

The scaling activity of Kcnk5b includes all the tissues of the entire appendages of the fish (Perathoner et al., 2014). Previous findings implicate broader intercellular electrophysiological gradients as a mechanism for tissue growth (Adams and Levin, 2013). Electrophysiological measurements of animal tissues show that electric fields are generated and are important *in vivo* (Borges et al., 1979; Jenkins et al., 1996; McGinnis and Jr., 1986), which suggests the existence of *in vivo* bioelectric information that regulates physiological phenomena. However, from our transplantation experiments, we observe that Kcnk5b's effect is cell autonomous (Fig. 3). Consequently, the question arises about how the activity of this K^+-leak channel relates to a broad, coordinated phenotype of scaling the several tissues of the fin. An answer is that the autonomous transcriptional programs include morphogens. What is unclear is whether a limited number of cells in the fin control the growth and organizing information so that Kcnk5b only needs to act on a limited number of cell types, or whether Kcnk5b regulates proportional growth at multiple levels and that the cell autonomous transcriptional response that we observe is one outcome of a combination of intracellular and intercellular responses induced by Kcnk5b.

Changes in membrane potential from alterations in K^+ conductance are also associated with the progression through the cell cycle (Blackiston et al., 2009; Urrego et al., 2014), because K^+ channel activity increases at specific cell cycle phases (Urrego et al., 2014), and inhibition of K^+ channel activity leads to cell cycle arrest in many different tissue cell types (Blackiston et al., 2009). It is possible that this phenomenon explains part of Kcnk5b's ability to promote allometric growth. We do not yet know whether other phenomena linked to the activity of mammalian Kcnk5 [influence cell tonicity (Niemeyer et al., 2010), metabolic acidosis and alkalinization (Warth et al., 2004), CO_2/O_2 chemosensing in retrotrapezoid nucleus neurons

(Flores et al., 2011) and apoptosis in lymphocytes and neurons (Göb et al., 2015; Nam et al., 2011)] are involved in appendage scaling.

We previously showed that calcineurin inhibition shifts isometric growth to allometric growth (Kujawski et al., 2014). Subsequently, Daane et al. showed that this effect is reversible in that removal of calcineurin inhibitors restores isometric growth. The authors also suggest an alternative mechanism for calcineurin regulation of Kcnk5b in its C-terminus (Daane et al., 2018); however, their model posits that active calcineurin promotes the activity of Kcnk5b, which does not yet explain how calcineurin inhibition and increased Kcnk5b activity each promote allometric growth (Kujawski et al., 2014; Perathoner et al., 2014). In either case, these data implicate calcineurin as a molecular switch governing isometric versus allometric growth control. Our findings provide a mechanism for how this switch acts to scale the fish appendages by directly regulating the activity of Kcnk5b through the dephosphorylation and phosphorylation of a specific serine (Fig. 7). The ability to mimic or block calcineurin regulation of this K^+-leak channel (Fig. 5), whose activity levels directly translate into the extent of allometric growth (Fig. 6), defines how calcineurin inhibition expands clonal populations during fin regeneration (Tornini et al., 2016). However, as we observed from both calcineurin inhibition (Kujawski et al., 2014) and from conditionally inducing Kcnk5b activity (Fig. 6), the induced allometric growth of the entire fin is more than expanding clonal populations, since the outcome is not tumorigenesis. Instead, the growth is coordinated among all the tissues (Fig. 6G-I,K,L) (Kujawski et al., 2014; Perathoner et al., 2014), and our finding that Kcnk5b activates several developmental pathways (Figs. 1,2,4) argues that calcineurin activity acting on Kcnk5b regulates more than cell cycle progression.

An important next step is to learn how the calcineurin-Kcnk5b circuit is integrated into the broader mechanisms that scale the appendages. Calcineurin is a Ca^{2+}-dependent enzyme which suggests that intracellular Ca^{2+} is involved in scaling information. Ca^{2+} is a broad second messenger that can activate several downstream Ca^{2+}-dependent enzymes, so broad changes in its subcellular levels likely have multiple effects. It remains unclear whether there is a specific intracellular distribution pattern that leads to calcineurin-mediated control of scaling. It is also possible that Ca^{2+}-mediated activation of calcineurin—and consequent restoration of isometric growth—is so dominant that other Ca^{2+}-mediated activities have little effect.

Two mechanisms that regulate proportional growth of organs are vitamin D and Hippo signaling. Increasing vitamin D signaling enhance the growth of the entire body, including the fins (Han et al., 2019). We propose that vitamin D is a systemic body signal that ultimately

leads to the increase in Kcnk5b signaling. It is also possible that this hormone acts independently of Kcnk5b. In *Drosophila*, the Hippo pathway regulates brain size and size of the imaginal discs (Poon et al., 2016; Rogulja et al., 2008). Mice overexpressing a nuclear version of the Hippo-signaling component Yap1 in the adult liver develop significantly enlarged livers (Camargo et al., 2007; Dong et al., 2007). The Hippo signal transduction pathway consists of several core components that can be regulated by different factors at plasma membrane and within the cell (Yu and Guan, 2013), so there are several possible nodes of interaction between of Kcnk5b and Hippo cascade. It is also possible the Hippo-mediated transcription regulates *kcnk5b* expression or channel activity.

Connexin43 also regulates proportional growth of the fins, since mutations that reduce the intercellular connectivity of connexin43 produce adult fins that are half the size as the fins of wild-type siblings (Hoptak-Solga et al., 2007; Iovine et al., 2005). The connective nature of these intercellular junction proteins indicate that direct communication between intracellular compartments of tissue cells is an important component of the scaling mechanism of the fins. Our observation that Kcnk5b cell-autonomously activates the *7XTCF-Xla.sam*:mCherry reporter (Fig. 3) indicates that it is not due to intracellular transfer of K^+. It is still unclear whether the disruption of intracellular trafficking of other ions (such as Na^+ or Ca^{2+}) or of other factors is responsible for the connexin43's effect on scaling.

Kcnk5b's ability to activate the Lef1-dependent reporter cell autonomously in different tissue types supports the conclusion that K^+ conductance has the potential to regulate developmental transcription in a broad range of tissues (Fig. 3B-E). The observation that neuronal cells in the brain and myocytes in the trunk muscle respond similarly to non-excitable cells elsewhere in the body suggests that even cells that harbor action potentials use K^+ conductance to regulate gene expression. However, when we either stably expressed or transient transfected Kcnk5b in different cell lines, we did not observe consistent activation of Lef1 or Shh (Fig. 4). We posit that the competencies of the cultured cell lines are different from the developmental competencies of the *in vivo* cells. Also, the mammalian cell lines are cancer cells, so they may already have an increased transcriptional base line for the selected developmental genes that the two-pore potassium-leak channels can only partially affect.

While we observed similarities between Kcnk5b and Kcnk9 or Kcnk10 in HEK cells, in Hela and N2A cells, we observed only partially similar profiles for the selected genes (while Kcnk9 and Kcnk10 were similar) (Fig. 4). We postulate that the observed differences may come from one or both of the following explanations. First, different responses from channels of the

same ion-type are due to different levels of membrane potential changes, which results in different levels of gene transcription. Second, these channels have different intracellular sequences, which may determine other unknown intermolecular interactions that have different signal transduction properties. In any case, we did observe that transgenic overexpression of Kcnk9 produces a similar allometric growth of the caudal fin (Fig. 6K,L). It remains to be explored whether intermolecular interactions between the channels and another protein contribute to the scaling of other organs as well as how other electrophysiological mechanisms that control membrane potential have the same growth effect.

In conclusion, we show how a specific electrophysiological mechanism activates important morphogen pathways to scale tissues in different *in vivo* contexts. We propose the observed diversity in morphogen and growth factor expression to Kcnk5b activity explains why the increased activity of Kcnk5b produces the diverse transcriptional response in the different tissues associated with the observed coordinated outgrowth of the entire fin. Also, we show how changes in phosphorylation of S345 in the cytoplasmic C-terminus can be regulated by calcineurin to directly control electrophysiological activity of the channel to scale the fin. Thus, we offer an *in vivo* paradigm in which membrane potential acts as potent regulator of coordinated developmental signaling, and we show how the two-pore K^+-leak channel Kcnk5b is involved in the initial activation of specific developmental mechanisms that lead to the scaling of the fish fin appendages.

Acknowledgements:

This work was supported by funding from ShanghaiTech University, and from the Deutsche Forschungsgemeinschaft Grant AN 797/4-1 (CLA). We thank the Microscope Facility of the School of Life Sciences and Technology at Shanghaitech University for their expertise and support. We also wish to thank C. Bökel for scientific discussions.

Competing Interests

The authors declare that there are no competing interests.

Figures

Figure 1: Kcnk5b induces a partial developmental gene response in uninjured adult fins.

(**A**) qRT-PCR results of *shh* and *lef1, aldh1α2*, *pea3* and *msxb* expression from caudal fins of 6-month-old wild-type (AB) and Tg[*hsp70*:*kcnk5b*-GFP] zebrafish 6 hours after heat shock (HS)of the caudal fins. (**B**) qRT-PCR results of *shh* and *lef1, aldh1α2*, *pea3* and *msxb* expression from caudal fins of 6-month-old wild-type (AB) and Tg[*hsp70*:*kcnk5b*-GFP] zebrafish 12-hours after heat-shock induction of the the caudal fins. (**C**) qRT-PCR results for GFP from the transgenic fish line Tg[*hsp70*:*kcnk5b*-GFP] at the indicated time points relative to the single heat-shock pulse of AB wild-type and transgenic fish. AB HS for each time point were always set at 1-fold, so they are represented as only one group in the graph. (**D**) qRT-PCR results for several genes in the caudal fin from daily heat-shock pulse of AB wild-type and Tg[*hsp70*:*knck5b*-GFP] over 3 days. (**E**) *in situ* hybridization experiments on fins show expression of *shh* (**a,b**) and *lef1* (**c,d**) in heat-shocked non-transgenic control fish (**a,c**) and heat-shocked Tg[*hsp70*:*kcnk5b*-GFP](**b,d**). (**F**) Cross sections through fin rays show expression of *lef1*(**a,b**) and *shh* (**c,d**) before (**a,c**) and after (**b,d**) heat-shock induction of Tg[*hsp70*:*kcnk5b*-GFP]. (**G**) Representative images of Western blots show expression of Shh, Lef1 and β-catenin before and 3 days after 10-minute daily heat-shock induction of *kcnk5b*-GFP in the fin. (**H**) Graphed measurements results of Western blots. (**I**) Confocal planes (0.45 μm) of immunohistochemistry stained 10 μm sections of control (no heat shock) or transgene-induced (heat shock) uninjured fins for merged GFP from Tg[*hsp70*:*kcnk5b*-GFP] and β-catenin (red) (**a-d**: Merged), GFP from Tg[*hsp70*:*kcnk5b*-GFP] (**e,f**: green) β-catenin (**g,h**: red) and DAPI (**i,j**: blue)of fin cross sections of transgenic Tg[*hsp70*:*kcnk5b*-GFP] animals without heat shock (**a,c,e,g,i**) or after heat shock (**b,d,f,h,j**). White boxes in **a** and **b** show location of magnified panels of **c,e,g** and **d,f,j**, respectively. Overlapping DAPI and β-catenin staining indicated by white arrows. Epi." refers to the outer multilayered epidermis, "Be." as the underlying basal epithelial layer, and "Mesen." refers to the underlying mesenchymal tissues. (**J**) Graphed measurements of DAPI stained nuclei containing staining of β-catenin. (**K**) qRT-PCR results for the indicated genes in the caudal fin from AB non-transgenic and Tg[*hsp70*:*knck5b*-GFP] fish after daily heat-shock pulses over 3 days. Scale bars are 50 μm (D), 1 mm (E), 10 μm (H). The data for each experiment represent 3 or more separate experiments. The data points show all technical replicates. Student's T-test used for the tests of significance between indicated experimental groups.

Figure 2: Kcnk5b induces *shh* and *lef1* in zebrafish larva.

(**Aa,b**) Comparison of gene expression from mRNA isolated from complete 3 dpf zebrafish larva harboring Tg[*hsp70*:*knck5b*-GFP] 6 hours after heat-shock (HS) induction. (**B**) *in situ* hybridization experiments on 2 dpf embyros for *shh* start to detect expression in the cells of the zone of polarity in the early pectoral fin bud by 60 minutes of incubation of the final staining reaction (**a-d**) or after overnight staining (**e-h**). Measurements of *shh* expression levels by computer-program-based detection of pixel level intensities (**i**) or by the stained area (**j**) in the early pectoral fin bud. Panels c,d,g,h are enlarged regions (open black boxes) in panels a,b,e,f. Arrows indicate *shh* expression in the developing fin buds. (**C**) Double transgenic 3dpf larva harboring Tg[*hsp70*:*kcn5b*-GFP] and hemizygous Tg[*7XTCF-Xla.sam*:mCherry] either before heat shock (**a-c**) or 12 hours after heat shock (**d-f**). (**Cg**) Measurements of mCherry intensity levels of non-transgenic (non-tg), *kcnk5b*-transgenic (*kcnk5b*) fish and transgenic fish harboring the Lef-1-dependent Tg[*7XTCF-Xla.sam*:mCherry] reporter (7xTCF) before and 12 hours after heat shock. (**D**) Cross sections through the trunks of non-transgenic (**a-d**) and Tg[*7XTCF-Xla.sam*:mCherry] (**e-h**) and Tg[*hsp70*:*kcn5b*-GFP]; Tg[*7XTCF-Xla.sam*:mCherry] double-transgenic (**i-l**) fish lines after heat shock. (**D**) Measurements from dorsal to ventral of the caudal finfold of Tg[*7XTCF-Xla.sam*:mCherry] and Tg[7XTCF-Xla.sam:mCherry] X Tg[*hsp70:kcnk5b*-GFP] sibling larva after heat shock. (**E**) Diagram of the measurement axes of the larva. (**F**) Length measurements from anterior-most point of the caudal finfold to its distal-most tip of 5 dpf larva. (**G**) Length measurements of the caudal finfold from the dorsal-most point to the ventral-most tip of 5 dpf larva. (**H**) Finfold anterioposterior length-to-body ratios of the caudal finfold of 5 dpf larva. (**I**) Finfold dorsoventral length-to-body ratios of the body ratios. (**J**) Body length measurements of 5 dpf larva as diagramed in (E). Scale bars are 100µm (**B,C**) and 20µm (**D**). The data for each panel represent 3 or more experiments. The data points show all technical replicates. Student's T-test used for all test of significance between the indicated experimental groups.

Figure 3: Kcnk5b induces Lef-1-dependent transcription in several tissues in a cell autonomous manner.

(**A**) Diagram of transplantation procedure and possible cell-autonomous and non-cell-autonomous outcomes on the expression of the Tg[*7XTCF-Xla.sam:mCherry*] Lef1 reporter after heat-shock induction of the Tg[*hsp70*:*kcnk5b*-GFP] transgene. (**B**) Transplantation experiments of donor cells from double transgenic fish harboring Tg[*hsp70*:*kcnk5b*-GFP] and Tg[7XTCF-Xla.sam:mCherry] into homozygous host embryos harboring only the Tg[7XTCF-Xla.sam:mCherry]. The head (**a**) eye (**e**) trunk (**i**) and finfold (**m**) of mosaic larva before heat shock induction of *kcnk5b*-GFP expression. Head (**b-d**), eye (**f-h**), trunk (**j-l**) and finfold (**n-p**) of 72 dpf larva at 24 hours after heat shock. (**C**) Bright field images of the head (**a,d**), jaw area (**g**) border tissue of otic vesicle (**j**) and trunk (**o,r**) of 72 hpf larva; GFP expression from Tg[*hsp70*:*kcnk5b*-GFP](**b,e,h,k,p,s**) and mCherry expression from Tg[*7XTCF-Xla.sam*:mCherry](**c,f,i,l,q,t**). (**D**) Higher magnification of merged (**a**) and separate GFP (**b**) and mCherry (**c**) channels of cells in the neural tube of 48 hpf embryos. Z-stack composite three-dimensional images before rotation (**d**), rotated 90º (**e**) and 180º (**f**). (**E**)Total number of positive cells counted in the tissues of all mosaic larva for all mCherry-positive cells from recipient Tg[*7XTCF-Xla.sam*:mCherry] larva, all GFP-positive cells from Tg[*hsp70*:*kcnk5b*-GFP](open green triangle) and all double positive cells (open blue squares). The data for each experiment represent 3 or more experiments with 2 or more biological replicates. Scale bars are equal to 200 µm (Ba-l), 50 µm (Bm-p), 20 µm (C) and 25 µm (D).

Figure 4: Kcnk5b channel activity regulates developmental gene transcription in mammalian cells.

(**A**) FRET-FLIM images after measuring the life time of CFP of the K^+ FRET reporter KIRIN (Shen et al., 2019). The color images indicate the differences in CFP fluorescence lifetime of the K^+ FRET reporter KIRIN in HEK293T (HEK) cells. Assigned rainbow of colors in the delineated cytoplasm depict the range of numeric values of nanoseconds (ns) of the detected fluorescent lifetime for CFP. Red represents longer lifetime values. Blue represents shorter lifetime values, and the other colors represent intermediary lifetime values. (**a**) Composite image of all lifetime values of the KIRIN K^+ reporter in control cells transfected with mCherry. (**b**) Image of low lifetime values in a control cell. (**c**) Image of high lifetime values in a control cell. (**d**) Composite image of all lifetime values of the KIRIN K^+ reporter in cells expressing *kcnk5b*-mCherry. (**e**) Image of low lifetime values in cells expressing *kcnk5b*-mCherry. (**f**) Image of high lifetime values in cells expressing *kcnk5b*-mCherry. (**g**) Compared to GFP-transfected HEK cells, cells transfected with *kcnk5b*-mCherry show an increase in CFP lifetime due to reduction in intracellular K^+. (**Ba**) qRT-PCR for SHH and LEF1 in HEK cells. (**Bb**) qRT-PCR for ALDH1a2, PEA3 and MSX1 in HEK cells. **(C**) qRT-PCR for indicated genes in HEK cells expressing GFP, *kcnk9*-GFP or *kcnk10*-GFP 24 hours after transfection. (**D**) qRT-PCR results in HeLa cells expressing either GFP or *kcnk5b*-GFP 24 hours after transfection. (**E,F)** qRT-PCR results in N2A cells expressing either GFP or *kcnk5b*-GFP 24 hours after transfection. (**G**) qRT-PCR results in Mcf7 cells expressing either GFP or *kcnk5b*-GFP 24 hours after transfection. (**H,I**) qRT-PCR measurement of indicated gene after 24 hour transfection of Kcnk9 in Hela cells. (**J**) qRT-PCR measurement of indicated gene after 24 hour transfection of Kcnk10 in Hela cells. (**K**) qRT-PCR measurement of indicated gene after 24 hour transfection of Kcnk9 in N2A cells. (**L**) qRT-PCR measurement of indicated gene after 24 hour transfection of Kcnk10 in N2A cells. The data represent 3 or more experiments, The data points show all technical replicates. Student's T-test was used for tests of significance and the levels of significance are indicated between the experimental groups.

Figure 5: Calcineurin functionally interacts and regulates channel activity of Kcnk5b. (**A**) Diagram of hypothetical interaction between Calcineurin (CaN) and Kcnk5b at a consensus calcineurin binding site (LVIP) in Kcnk5b. (**B**) Whole-cell patch clamp of HEK293T (HEK) cells expressing the indicated zebrafish proteins: Calcineurin-mCherry and Kcnk5b-GFP. (**C**) Whole-cell patch-clamp results of cells expressing zebrafish Kcnk5b-GFP and treated either with DMSO or the calcineurin inhibitor FK506. (**D**) Diagram shows mutant Kcnk5b with altered amino acids at putative calcineurin binding site and graph of the Patch-clamp results of the wild-type zebrafish Kcnk5b channel (Kcnk5bLVIP) or mutant Kcnk5b (Kcnk5bmutVATA) lacking the putative calcineurin binding site. Each construct is expressed either with or without calcineurin (CaN). (**E)** qRT-PCR for SHH in HEK cell lines stably expressing either GFP or Kcnk5b-GFP and transfection with calcineurin-mCherry (CaN). **(F**) qRT-PCR for PEA3 in HEK cell lines stably expressing either GFP or Kcnk5b-GFP and transfection with calcineurin-mCherry (CaN). (**G**) qRT-PCR of SHH expression HEK cells after transfection either with GFP, *kcnk9*-GFP or *kcnk10*-GFP with or without calcineurin (CaN). (**H**) qRT-PCR of PEA3 expression HEK cells after transfection either with GFP, *kcnk9*-GFP or *kcnk10*-GFP with or without calcineurin (CaN). The electrophysiology measurements (**B-D**) are averages with SEM. (**E-G**) Graph panels show averages. The data represent 3 or more experiments. The averaged data points graphed in D-B have 2 or more technical replicates per experiment. The data points graphed in E-H show all technical replicates. Student's T test was used to determine the indicated significance (P) values.

699 **Figure 6: Regulation of Kcnk5b controls scaling of the fin.**

700 (**A**) Diagram of Kcnk5b channel showing proposed Serine345Proline346 calcineurin
701 dephosphorylation site adjacent the calcineurin-interaction site (LVIP). Mutation of S345 to
702 alanine (A) mimics dephosphorylation. (**B)** Whole-cell patch-clamp results of HEK239T (HEK)
703 cells transfected with zebrafish wild-type channel (Kcnk5bS345) or the dephospho-mimic
704 mutant (KcnkS345A) either with or without calcineurin (CaN). (**C**) Diagram of serine (S) to
705 glutamic acid (E) substitution to mimic phosphorylation of Kcnk5b. (**D**) Whole-cell patch-
706 clamp measurements for wild-type Kcnk5b and mutant Kcnk5b harboring a Serine345 to
707 glutamic acid either with or without calcineurin (CaN). (**E**) Graph displays different growth
708 rates of the regenerating caudal fin lobes of the indicated transgenic fish lines. Body length of
709 each fish was used to standardize the fin length measurements (fin-to-body ratio). (**F**) Caudal
710 fin of Tg[*hsp70:kcnkbS345A*] transgenic fish after regeneration of ventral lobe. (**G**) Caudal fin
711 of Tg[*hsp70:kcnk5bS345*] transgenic fish after regeneration of ventral lobe. (**H**) Caudal fin of
712 Tg[*hsp70:kcnk5bS345E*] transgenic fish after regeneration of ventral lobe. (**I**) Graph of fin-to-
713 body ratios of the unamputated lobes of the indicated transgenic fish lines at 33 days of the
714 same fish as in (F). (**J**) Representative caudal fins of the Tg[*hsp70*:*kcnk9*-GFP] fish that was
715 allowed to regenerate without any heat-shock induction of the transgene (**a**) or underwent a
716 daily 10 min heat-shock induction of the Tg[*hsp70*:*kcnk9*-GFP] transgene (**b**). (**K**) Assessment
717 of regenerative fin growth at 33 dpa of the indicated fish lines and heat-shock treatment. The
718 data for each experiment represent 3 or more experiments. The averaged data points in B,D,E
719 represent 2 or more technical replicates per experiment. The graphed data in I,K show all
720 technical replicates. The electrophysiology measurements (panels **B,D**) are represented as
721 averages with SEM. Significance values shown in the graphs were measured by students t-tests
722 (E, I, K) are represented as averages and SD. The scale bars equal 2 mm (F-H,Ja,b). Arrows
723 and dashed lines in F-H,Ja,b indicate amputation planes through fins.

724

Figure 7: Model of calcineurin regulation of Kcnk5b-mediated activation of developmental gene transcription. Kcnk5b activation results in reduced cytoplasmic K^+, which is sufficient to induce the transcription of the *shh* ligand and *lef1* transcription factor as well as components of other developmental pathways to induce coordinated allometric growth of the tissues of the fish fin appendage. Scaling information from the body or local tissues in the fin activate calcineurin so that it dephosphorylates Kcnk5b on S345 to reduce its K^+-channel activity, which results in isometric growth of the fin.

Supplementary Figure Legends:

Figure 1-Supplementary Figure 1: Induction of developmental genes after induction of *kcnk5b* expression.

(**A**) (**A**) qRT-PCR results of *shh* and *lef1* expression from caudal fins of 6-month-old zebrafish comparing before (-HS) and 6 hours after (+HS) heat shock induction of the Tg[*hsp70*:*kcnk5b*-GFP] transgene in the caudal fins. (**B**) Confocal image of immunohistochemistry staining for GFP expression in a cross section of the distal tip of the adult fin after heat shock induction of *kcnk5b*-GFP in a fish harboring the Tg[*hsp70*:*kcnk5b*-GFP] transgene. The lower left inset is an enlarged view of the expression of the transgene in the fin. (**C**) Confocal image of DAPI-stained nuclei of the same confocal section in panel A. (**D**) Overlay of the confocal GFP and DAPI images. **E**) qRT-PCR results for the indicated genes in the caudal fin from AB non-transgenic and Tg[*hsp70*:*knck5b*-GFP] fish after daily heat-shock pulses over 3 days. (**F**) qRT-PCR for GFP expression in AB wild-type strain fish and kcnk5b-GFP fish after daily heat-shock pulses over 3 days. () The data for each panel represents 3 or more experiments. The graphed data points show all technical replicates.

Figure 1-Supplementary Figure 2: Protein expression of selected developmental genes and β-catenin subcellular distribution.

(**A**) Example blot for Shh expression in adult fins with or without heat-shock induction of the Tg[*hsp70*:*kcnk5b*-GFP] transgene. (**B**) Example blot for Lef1 expression in adult fins with or without heat-shock induction of the Tg[*hsp70*:*kcnk5b*-GFP] transgene. (**C**) Example blot for β-catenin expression in adult fins with or without heat-shock induction of the Tg[*hsp70*:*kcnk5b*-GFP] transgene. (**D**) Example blot for β-actin expression in adult fins with or without heat-

shock induction of the Tg[*hsp70*:*kcnk5b*-GFP] transgene. (**E-G**) Three adjacent serial confocal sections through the fin of a control non-heat-shocked Tg[*hsp70*:*kcnk5b*-GFP] fish. Dapi stains the nuclei (blue) and immunohistochemistry for β-catenin (red). (**a**) Lower magnifications. (**b**) Corresponding higher magnifications for each preceding (a) panel. (**H-J**) Three adjacent serial confocal sections through the fin of a heat-shocked Tg[*hsp70*:*kcnk5b*-GFP] fish. Dapi stains the nuclei (blue) and immunohistochemistry for β-catenin (red). (**a**) Lower magnifications. (**b**) Corresponding higher magnifications for each preceding (a) panel. (**K**) Graphed measurements of β-catenin fluorescence intensity of stained sections. All scale bars are equal to 10 μm. The data for each panel represent 3 or more experiments. The graphed data points show all technical replicates

Figure 2-Supplementary Figure 1: Controls for shh expression and transgenic expression of Kcnk5b in embryos. (**A**) Transgenic expression of Kcnk5b after single heat shock pulse induces transgene expression. (**B**) *in situ* probe for *shh* shows expected expression pattern. (**C**) Ratios of finfold and body length measurements of caudal finfold along the anterioposterior axes of 3 dpf single transgenic Tg[*7XTCF-Xla.sam*:mCherry] and double transgenic Tg[*7XTCF-Xla.sam*:mCherry] X Tg[*hsp70*:*kcnk5b*-GFP] after 3x once-a-day heat-shock pulse, 30 min each. Each panel represents 3 or more experiments. The graphed data show all technical replicates.

Figure 3-Supplementary Figure 1: Expression of Kcnk5b-GFP from Tg[*hsp70*:*kcnk5b*-GFP] after single heat shock and consequent activation of *7XTCF-Xla.sam*:mCherry**.**

(**A**) Representative bright field cross section through the mid-section of heat-shocked transgenic zebrafish 72 hpf larva. (**B**) Immunohistochemical staining for GFP of the same cross section in panel A. (**C**) DAPI staining of the same cross section in panel A. (**D**) Representative confocal image of immunohistochemical staining for GFP in heat-shocked transgenic zebrafish larva showing membranous staining of Kcnk5b-GFP. (**E**) DAPI staining of the same confocal section in panel D. (**F**) Merged image of panels D and E.. (**Ga-i**) Images of cells in the head 48 hpf embryos expressing *kcnk5*b-GFP transgene and mCherry from the *7XTCF-Xla.sam*:mCherry transgene. (**a**) Bright fish image, (**b**) merge of GFP and mCherry, (**c**) enlargement of (b), (**d**) GFP image, (**e**) enlargement of (d), (**f**) mCherry image, (**g**) enlargement of (f), (**h**) 3D composite of z-stacked images, (**i**) enlargement of (h). (**Ha-i**) Images of cells in the brain of 48 hpf embryos expressing *kcnk5b*-GFP transgene and mCherry from the *7XTCF-Xla.sam*:mCherry transgene.

(**a**) Bright fish image, (**b**) merge of GFP and mCherry, (**c**) enlargement of (b), (**d**) GFP image, (**e**) enlargement of (d), (**f**) mCherry image, (**g**) enlargement of (f), (**h**) 3D composite of z-stacked images, (**i**) enlargement of (h). (**Ia-i**) Images of cells in the developing otic vesical of 48 hpf embryos expressing kcnk5b-GFP transgene and mCherry from the 7XTCF-Xla.sam:mCherry transgene. (**a**) Bright fish image, (**b**) merge of GFP and mCherry, (**c**) enlargement of (b), (**d**) GFP image, (**e**) enlargement of (d), (**f**) mCherry image, (**g**) enlargement of (f), (**h**) 3D composite of z-stacked images, (**i**) enlargement of (h). (**Ja-i**) Images of cells in the developing neural tube of 48 hpf embryos expressing *kcnk5b*-GFP transgene and mCherry from the *7XTCF-Xla.sam*:mCherry transgene. (**a**) merge of GFP and mCherry, (**b**) enlargement of (a), (**c**) eGFP image, (**d**) enlargement of GFP image (c), (**e**) mCherry image, (**f**) enlargement of mCherry image (e), (**g**) 3D composite of z-stacked images, (**h**) enlargement of 3D composite (g), (**i**) 90º rotation of 3D composite of z-stacked images (g). Scale bars equal 40 µm (A-C), 5 µm (D-F), 20 µm (G-J). The data for each panel represents 3 or more experiments.

Figure 4-Supplementary Figure 1: Expression and activity of Kcnk5b-GFP in transfected HEK293T cells.

(**A**) Confocal image of through an immunocytochemical staining of a HEK293T cell transfected with zebrafish *kcnk5b*-GFP transgene (**B**) DAPI staining of the same cell in panel A. (**C**) Merged panels A and B. (**D-L**) Serial confocal cross sections for GFP in a live HEK293T cell from its surface (**D**) through to a mid-section of the cell (**L**) after transfection with the zebrafish *kcnk5b*-GFP transgene. (**M**) FRET-FLIM image after measuring the life time of CFP of the K^+ FRET reporter KIRIN in a cell transfected with a control plasmid only expressing mCherry. The inset image of the confirmation of the FRET reporter depicting how FRET occurs. (**N**) FRET-FLIM image after measuring the life time of CFP of the K^+ FRET reporter KIRIN in a cell transfected with a plasmid expressing *kcnk5b*-mCherry. The inset image of the confirmation of the FRET reporter depicting how FRET do not occur. (**O**) The graphed assessments of the changes in CFP lifetime in the control mCherry-expressing cells and the cells expressing *kcnk5b*-mCherry. The diagrams to the right of the graph depict the conformational changes that result in the values of the lifetimes of CFP. The data for each experiment represents 3 or more experiments. The graphed data points show all technical replicates.

Figure 4-Supplementary Figure 2: Comparison of Kcnk5b with Knck9 or with Kcnk10.

(**A,B**) qRT-PCR measurement of the indicated gene after 24 hour transfection of Kcnk5b in HEK293T cells. (**C,D**) Comparison between zebrafish amino acid sequences from Kcnk5b (blue) and Kcnk9 (C, black) and Kcnk10b (D, black) show conserved (red letter) and similar properties (red plus sign) amino acids. Yellow-highlighted letters indicate calcineurin binding site, and green-highlighted letters indicate the site of post-translational modification by calcineurin. The data for each experiment represent 3 or more experiments. The graphed data points show all technical replicates.

Figure 6-Supplementary Figure 1: Activity measurements of Kcnk5b Serine mutant channels

(A) Diagram of Kcnk5b channel showing proposed Serine345 calcineurin dephosphorylation site (yellow) adjacent the calcineurin-interaction site (LVIP). Two other serines (blue) were substituted with alanines or glutamic acids to mimic dephosphorylation or phosphorylation. (**B**) Electrophysiology measurements of wild-type Kcnk5b (blue) and serine-to-alanine mutant Kcnk5bS330A (purple). **(C)** Electrophysiology measurements of wild-type Kcnk5b (blue) and serine-to-alanine mutant Kcnk5bS332A (yellow). **(D)** Electrophysiology measurements of wild-type Kcnk5b (blue) and serine-to-alanine mutant Kcnk5bS345A (orange). **(E)** Electrophysiology measurements of wild-type Kcnk5b (blue), serine-to-glutamic acid mutant Kcnk5bS330E (black) and Kcnk5bS330E plus calcineurin (CaN) (red). **(F)** Electrophysiology measurements of wild-type Kcnk5b (blue), serine-to-glutamic acid mutant Kcnk5bS332E (black) and Kcnk5bS332E plus calcineurin (CaN) (red). (**G**) Body length measurements from tip of the head to the base of the fin for each transgenic fish are represented as averages and standard deviation. (**H**) Body length measurements from tip of the head to the base of the fin for each fish of either wild-type (AB) or Tg[*hsp70*:*kcnk9*-GFP] (*kcnk9*) either without (–HS) or with (+HS) heat shock. The data for each experiment represent 3 or more experiments. The averaged data points in B-G represent 2 or more technical replicates per experiment. The data in H show all technical replicates.

References:

Adams, D.S., and Levin, M. (2013). Endogenous voltage gradients as mediators of cell-cell communication: strategies for investigating bioelectrical signals during pattern formation. Cell Tissue Research *352*, 95-122.

Andersen, E.D., Krasilnikoff, P.A., and Overvad, H. (1971). Intermittent muscular weakness, extrasystoles, and multiple developmental anomalies. A new syndrome? Acta Paediatr Scand *60*, 559-564.

Baer, M.L., and Colello, R.J. (2016). Endogenous bioelectric fields: a putative regulator of wound repair and regeneration in the central nervous system. Neural Regneration Research *11*, 861-864.

Balciunas, D., Wangensteen, K.J., Wilber, A., Bell, J., Geurts, A., Sivasubbu, S., Wang, X., Hackett, P.B., Largaespada, D.A., McIvor, R.S., *et al.* (2006). Harnessing a high cargo-capacity transposon for genetic applications in vertebrates. PLoS Genetics *2*, e169.

Bartel, D.P., Sheng, M., Lau, L.F., and Greenberg, M.E. (1989). Growth factors and membrane depolarzation activate distinct programs of early response gene expressoin: dissociation of fos and jun induction. Genes & Development *3*, 304-313.

Blackiston, D.J., McLaughlin, K.A., and Levin, M. (2009). Bioelectric controls of cell proliferation: Ion channels, membrane voltage and the cell cycle. Cell Cycle *8*, 3527-3536.

Borgens, R.B., J. W. Vanable, J., and Jaffe, L.F. (1977). Bioelectricity and Regeneration. I Initiation of Frog Limb Regeneration by Minute Currents. Journal of Experimental Zoology *200*, 403-416.

Borges, R.B., Joseph W. Vanable, J., and Jaffe, L.F. (1979). Reduction of Sodium Dependent Stump Currents Disturbs Urodele Limb Regeneration. Journal of Experimental Zoology *208*, 377-386.

Brand, M., Granato, M., and Nüsslein-Volhard, C. (2002). Keeping and raising zebrafish. In Zebrafish: a Practical Approach, C. Nüsslein-Volhard, and R. Dahm, eds. (Oxford University Press), pp. 7-38.

Camargo, F.D., Gokhale, S., Johnnidis, J.B., Fu, D., Bell, G.W., and al., e. (2007). YAP1 increases organ size and expands undifferentiated progenitor cells. Current Biology *17*, 2054-2060.

Canun, S., Perez, N., and Beirana, L.G. (1999). Andersen syndrome autosomal dominant in three generations. Am J Med Genet *85*, 147-156.

Cao, Z., Meng, Y., Gong, F., Xu, Z., Liua, F., Fang, M., Zou, L., Liao, X., Wang, X., Luo, L., *et al.* (2021). Calcineurin controls proximodistal blastema polarity in zebrafish fin regeneration. PNAS *118*, e2009539118.

Chow, R.L., Altmann, C.R., Lang, R.A., and Hemmati-Brivanlou, A. (1999). Pax6 induces ectopic eyes in a vertebrate. Development *126*, 4213-4222.

Daane, J.M., Lanni, J., Rothenberg, I., Seebohm, G., Higdon, C.W., Johnson, S.L., and Harris, M.P. (2018). Bioelectric-calcineurin signaling module regulates allometric growth and size of the zebrafish fin. Scientific Reports *8*, 10391.

Dahal, G.R., Rawson, J., Gassaway, B., Kwok, B., Tong, Y., Ptacek, L.J., and Bates, E. (2012). An inwardly rectifying K+ channel is required for patterning. Development *139*, 3653-3664.

Dong, J., Feldmann, G., Huang, J., Wu, S., Zhang, N., Comerford, S.A., Gayyed, M.F., Anders, R.A., Maitra, A., and Pan, D. (2007). Elucidation of a universal size-control mechanism in Drosophila and mammals. Cell *130*, 1120-1133.

Durant, F., Bischof, J., Fields, C., Morokuma, J., LaPalme, J., Hoi, A., and Levin, M. (2019). The role of early bioelectric signals in the regeneration of planarian anterior/posterior polarity. Biophysical Journal *116*, 948-961.

Emmons-Bell, M., and Hariharan, I.K. (2021). Membrane potential regulates hedgehog signaling in the Drosophila wing imaginal disc. EMBO Reports *e51861*.

Flores, C., Cid, L., Niemeyer, M., and Sepulveda, F. (2011). B Lymphocytes taken to task: a role for a background conductance K2p K+ channel in B cells. Focus on "Expression of TASK-2 and its up-regulation by B cell receptor stimulation in WEJI-231 mouse immature B cells". American Journal of Physiology Cell Physiology *300*, C976-C978.

Geremia, N.M., Gordon, T., Burshart, T.M., Abdulhakeem A. Al, M., and Verge, V.M.K. (2007). Electrical Stimulation Promotes Sensory Neuron Regeneration and Growth-associated Gene Exrpression. Experimental Neurobiology *205*, 327-359.

Göb, E., Bittner, S., Bobak, N., Kraft, P., Göbel, K., Langhauser, F., Homola, G.A., Brede, M., Budde, T., Meuth, S.G.*, et al.* (2015). The two-pore domain potassium channel KCNK5b deteriorates the outcome in ischemic neurodegeneration. Pfluger Archive-European Journal of Physiology *467*, 973-987.

Goldstein, S.A.N., Bockenhauer, D., O'Kelly, I., and Zilberberg, N. (2001). Potassium leak channels and the KCNK family of two-P-domain subuints. Nature Reviews Neuroscience *2*, 176-184.

Grigoriu, S., Bond, R., Cossio, P., Chen, J.A., Ly, N., Hummer, G., Page, R., Cyert, M.S., and Peti, W. (2013). The molecular mechanisms of substrate engagement and immunosuppressant inhibition of calcineurin. Plos Biology *11*, e1001492.

Halder, G., Callaerts, P., and Gehring, W.J. (1995). Induction of ectopic eyes by targeted expression of the eyeless gene in Drosophila. Science *267*, 1788-1792.

Han, Y., Chen, A., Umansky, K.-B., Oonk, K.A., Choi, W.-Y., Dickson, A.L., Ou, J., Cigiola, V., Yifa, O., Cao, J.*, et al.* (2019). Vitamin D stimulates cardiomyocyte proliferation and controls organ size and regeneration in zebrafish. Developmental Cell *48*, 853-863.

Hoptak-Solga, A.D., Klein, K.A., DeRosa, A.M., White, T.W., and Iovine, M.K.-. (2007). Zebrafish short fin mutations in connexin4 lead to aberrant gap junctional intercellular communication. FEBS letters *581*, 3297-3302.

Iovine, M.K., Higgins, E.P., Hindes, A., Coblitz, B., and Johnson, S.L. (2005). Mutations in *connextin43* (*GJA1*) perturb bone growth in zebrafish fins. Developmental Biology *278*, 208-219.

Jenkins, L.S., Duerstock, B.S., and Borges, R.B. (1996). Reduction of the Current of Injury Leaving the Amputation Inhibits Limb Regeneration in the Red Spotted Newt. Developmental Biology *178*, 251-262.

Kawakami, Y., Rodriguez Esteban, C., Raya, M., Kawakami, H., Marti, M., Dubova, I., and Izipisua Belmonte, J.C. (2006). Wnt/beta-catenin siganling regulates vertebrate limb regeneration. Genes & Development *20*, 3232-3237.

Kujawski, S., Lin, W., Kitte, F., Börmel, M., Fuchs, S., Arulmozhivarman, G., Vogt, S., Theil, D., Zhang, Y., and Antos, C.L. (2014). Calcineurin regulates coordinated outgrowth of zebrafish regenerating fins Developmental Cell *28*, 1-15.

Lanni, J.S., Peal, D., Ekstrom, L., Chen, H., Stanclift, C., Bowen, M.E., Mercado, A., Gamba, G., Kahle, K.T., and Harris, M.P. (2019). Integrated K+ channel and K+Cl- cotransporter function are required for the coordination of size and proportion during development. Dev Biol *456*, 164-178.

Levin, M. (2014). Molecular bioelectricity: how endogenous voltage potentials control cell behavior adn instruct pattern regualtion in vivo. Molecular Biology of the Cell *25*, 3835-3850.

Marcoux, A.A., Garneau, A.P., Frenette-Cotton, R., Slimani, S., Mac-Way, F., and Isenring, P. (2017). Molecular features and physiologal roles of K+-Cl- cotransporter 4. BBA-General Subjects *1861*, 3154-3166.

McCaig, C.D., Rajnicek, A.M., Song, B., and Zhao, M. (2005). Controlling Cell Behavior Electrically: Current Views and Future Potential. Physiol Rev *85*, 943-978.

McGinnis, M.E., and Jr., J.W.V. (1986). Electrical Fields in Notophthalmus viridescens Limb Stumps. Developmental Biology *116*, 184-193.

McLaughlin, K.A., and Levin, M. (2018). Bioelectric signaling in regeneration: Mechanismsof ionic controls of growth and form. Developmental Biology *433*, 177-189.

Messerli, M.A., and Graham, D.A. (2011). Extracellular electrical fields direct wound healing and regeneration. The Biological Bulletin *221*, 72-92.

Moro, E., Ozhan-Kizil, G., Mongera, A., Beis, D., Wierzbicki, C., Young, R.M., Bournele, D., Domenichini, A., Valdivia, L.E., Lum, L.*, et al.* (2012). In vivo Wnt signaling tracing through a transgenic biosensor fish reveals novel activity domains. Developmental Biology *366*, 327-340.

Morokuma, J., Blackiston, D., Adams, D.S., Seebohm, G., Trimmer, B., and Levin, M. (2008). Modulation of potassium channel functions confers a hyperproliferative invasive phenotype on embryonic stem cells. Proceeding of the National Academy of Sciences USA *105*, 16608-16613.

Nam, J., Shin, D., Zheng, H., Lee, D., Park, S., Park, K., and Kim, S. (2011). Expression of TASK-2 and its upregulation by B cell receptor stimulation in WEHI-231 mouse immature B cells. American Journal of Physiology Cell Physiology *300*, C1013-1022.

Niemeyer, M., Cid, L., Pena-Münzenmayer, G., and Sepulveda, F. (2010). Modulation of the two-pore domain acid-sensitive K+ channel TASK-2 (KCNK5) by changes in cell volume. Journal of Biological Chemistry *276*, 43166-43174.

Pai, V.P., Aw, S., Shomrat, T., Lemire, J.M., and Levin, M. (2012). Transmembrane voltage potential controls embryonic eye patterning in Xenopus laevis. Development *139*, 313-323.

Pai, V.P., Lemire, J.M., Chen, Y., Lin, G., and Levin, M. (2015). Local and long-range endogenous resting potential gradients antagonistically regulate apoptosis and proliferation in the embryonic CNS. International Journal of Developmental Biology *59*, 327-340.

Perathoner, S., Daane, J.M., Henrion, U., Seebohm, G., Higdon, C.W., Johnson, S.L., Nüsslein-Volhard, C., and Harris, M.P. (2014). Bioelectric signaling regulates size in zebrafish fins. PLoS Genetics *10*, e1004080.

Poon, C.L.C., Mitchell, K.A., Kondo, S., Cheng, L.Y., and Harvey, K.F. (2016). The hippo pathway regulates neuroblasts and brain size in Drosophila melanogaster. Current Biology *26*, 1034-1042.

Rogulja, D., Rauskolb, C., and Irvine, K.D. (2008). Morphogen control of Wing Growth troguh the fat signaling pathway. Developmental Cell *15*, 309-321.

Sansone, V., Griggs, R.C., Meola, G., Ptacek, L.J., Barohn, R., Iannaccone, S., Bryan, W., Baker, N., Janas, S.J., Scott, W.*, et al.* (1997). Andersen's syndrome: a distinct periodic paralysis. Ann Neurol *42*, 305-312.

Shattock, M.J., Ottolia, M., Bers, D.M., Blaustein, M.P., Boguslavskyi, A., Bossuyt, J., Bridge, J.H.B., Chen-Izu, Y., Clancy, C.E., Edwards, A.*, et al.* (2015). Na+/Ca2+ exchange and Na+/K+-ATPase in the heart. Journal of Physiology *593.6*, 1361-1382.

Shen, Y., Wu, S.-Y., Rancic, V., Aggarwal, A., Qian, Y., Miyashita, S.-I., Ballanyi, K., Campbell, R.E., and Dong, M. (2019). Genetically encoded fluorescent indicators for imaging intracellular potassium ion concentration. Communications Biology *2*.

Stewart, S., Bleu, H.K.L., Yette, G.A., Henner, A.L., Braunstein, J.A., and Stankunas, K. (2020). longfin causes *cis*-ectopic expression of the *kcnh2a ether-a-go-go* K+ channel to autonomously prolong fin outgrowth. bioRxiv

Stoick-Cooper, C.L., Weidinger, G., Riehle, K.J., Hubbert, C., Major, M.B., Fausto, N., and Moon, R.T. (2007). Distinct Wnt siganling pathways have opposing roles in appendage regeneration. Development *134*, 479-489.

Sundelacruz, S., Levin, M., and Kaplan, D.L. (2009). Role of Membrane Potential in the Regulation of Cell Proliferation and Differentiation. Stem Cell Review and Reports *5*, 231-246.

988 Tawil, R., Ptacek, L.J., Pavlakis, S.G., DeVivo, D.C., Penn, A.S., Ozdemir, C., and Griggs, R.C.
989 (1994). Andersen's syndrome: potassium-sensitive periodic paralysis, ventricular ectopy and
990 dysmorphic features. Ann Neurol *35*, 326-330.

991 Tornini, V.A., Puliafito, A., Slota, L.A., Thompson, J.D., Nachtrab, G., Kaushik, A.-L., Kapsimali,
992 M., Primo, L., Talia, S.D., and Poss, K.D. (2016). Live Monitoring of Blastema Cell Contributions
993 during Appendage Regeneration. Current Biology *26*, 2981-2991.

994 Urrego, D., Tomczak, A.P., Zahed, F., Stühmer, W., and Pardo, L.A. (2014). Potassium channels in
995 cell cycle and cell proliferation. Philosophical Transactions of the Royal Society B *369*, 20130094.

996 Warth, R., Barriere, H., Meneton, P., Bloch, M., Thomas, J., Tauc, M., Heitzmann, D., Romeo, E.,
997 Verrey, F., Mengual, R.*, et al.* (2004). Proximal renal tubular acidosis in TASK2 K+ channel-deficient
998 mice reveals a mechanism for stabilizing bicarbonate transport. Proceeding of the National Academy
999 of Scinences USA *101*, 8215-8220.

1000 Yasuda, I. (1974). Mechanical and Electrical Callus. Clinical Studies. Annals New York Academy of
1001 Sciences, 457-465.

1002 Yoon, G., Quitania, L., Kramer, J.H., Fu, Y.H., Miller, B.L., and Ptacek, L.J. (2006a). Andersen-Tawil
1003 syndrome: definition of a neurocognitive phenotype. Neurology *66*, 1703-1710.

1004 Yoon, G., Tristani-Firouzi, M., Etheridge, S.P., Quitania, L., Kramer, J.H., Miller, B.L., Fu, Y.H., and
1005 Ptacek, L.J. (2006b). Andersen-Tawil syndrome: prospective cohort analysis and expansion of the
1006 phenotype. Am J Med Genet *140A*, 312-321.

1007 Yu, F.-X., and Guan, K.-L. (2013). The Hippo pathway: regulators and regulations. Genes &
1008 Development *27*, 355-371.

1009 Zaritsky, J.J., Eckman, D.M., Wellman, G.C., Melson, M.T., and Schwarz, T.L. (2000). Targeted
1010 disruption of Kir2.1 and Kir2.2 genes reveals the essential role of the inwardly rectifying K(+) current
1011 in K(+) -mediated vasodilation. Circulation Research *87*, 160-166.

1012 Zhao, M., Pu, J., Forrester, J.V., and McCaig, C.D. (2002). Membrane lipids, EGF receptors, and
1013 intracellular signals colocalize and are polarized in epithelial cells moving directionally in a
1014 physiological electric field. FASEB Journal *16*.

1015

1016

1017 **Material and Methods**

Key Resources Table				
Reagent type (species) or resource	**Designation**	**Source or reference**	**Identifiers**	**Additional information**
gene (Danio rerio)	Kcnk5b	genebank	ZFIN:ZDB-GENE-040426-1297	
gene (Danio rerio)	Kcnk9	genebank	ZFIN:ZDB-GENE-070705-260	
gene (Danio rerio)	Kcnk10a	genebank	ZFIN:ZDB-GENE-041210-291	
gene (Homo sapiens)	CaN	genebank	HGNC:HGNC:9314	
gene (Danio rerio)	lef1	genebank	ZFIN:ZDB-GENE-990714-26	
gene (Danio rerio)	shha	genebank	ZFIN:ZDB-GENE-980526-166	
gene (Danio rerio)	aldh1a2	genebank	ZFIN:ZDB-GENE-011010-3	
gene (Danio rerio)	pea3	genebank	ZFIN:ZDB-GENE-990415-71	
gene (Danio rerio)	msxb	genebank	ZFIN:ZDB-GENE-980526-312	

gene (Danio rerio)	ptch1	genebank	ZFIN:ZDB-GENE-980526-196	
gene (Danio rerio)	ptch2	genebank	ZFIN:ZDB-GENE-980526-44	
gene (Danio rerio)	bmp2b	genebank	ZFIN:ZDB-GENE-980526-474	
gene (Danio rerio)	axin2	genebank	ZFIN:ZDB-GENE-000403-2	
gene (Danio rerio)	bactin2	genebank	ZFIN:ZDB-GENE-000329-3	
gene (Homo sapiens)	lef1	genebank	HGNC:HGNC:6551	
gene (Homo sapiens)	shh	genebank	HGNC:HGNC:10848	
gene (Homo sapiens)	aldh1a12	genebank	HGNC:HGNC:15472	
gene (Homo sapiens)	pea3	genebank	HGNC:HGNC:3493	
gene (Homo sapiens)	msxb	genebank	HGNC:HGNC:7391	

gene (Homo sapiens)	GAPDH	genebank	HGNC:HGNC:4141	
strain, strain background (AB as background, both male and female)	Tg[hsp70:Kcnk5b-GFP]	AB fish from CZRC	AB fish Catlog ID: CZ1	Based on tol2 transposable element
strain, strain background (AB as background, both male and female)	Tg[hsp70:Kcnk5b S345A-GFP]	AB fish from CZRC	AB fish Catlog ID: CZ1	Based on tol2 transposable element
strain, strain background (AB as background, both male and female)	Tg[hsp70:Kcnk5b S345E-GFP]	AB fish from CZRC	AB fish Catlog ID: CZ1	Based on tol2 transposable element
strain, strain background (AB as background, both male and female)	Tg[hsp70:Kcnk9-GFP]	AB fish from CZRC	AB fish Catlog ID: CZ1	Based on tol2 transposable element
strain, strain background (AB as background, both male and female)	Tg[7XTCF-Xla.sam:mCherry]	European Zebrafish Resource Center	Cat.#:15200	
genetic reagent (Oryzias latipes)	Transposase RNA	This paper	This paper	In vitro transcripted by sp6 kit
genetic reagent	DIG RNA Labeling Mix	Roche	Cat.#:12770073	
genetic reagent (E. coli)	T7 RNA-polymerase	Promega	Cat. #:P207B	
cell line (human)	pLenti-CMV-	OBiO	Contract number:HYKY-	Titer:1.67E*08 TU/ml

	Kcnk5b-EGFP		181108018-DLV	
cell line (human)	pLenti-CMV-EGFP	OBiO	Contract number:HYKY-181108018-DLV	Titer:1.55E*09 TU/ml
transfected construct (human)	CMV-Kcnk5b-GFP	this paper	primers from https://www.genewiz.com.cn	Kcnk5b is cloned from adult zebrafish fin cDNA library
transfected construct (human)	CMV-Kcnk9-GFP	this paper	primers from https://www.genewiz.com.cn	Kcnk9 is cloned from zebrafish 3dpf larva cDNA library
transfected construct (human)	CMV-Kcnk10-GFP	this paper	primers from https://www.genewiz.com.cn	Kcnk10 is cloned from zebrafish 3dpf larva cDNA library
transfected construct (human)	CMV-CaN-Mcherry	this paper	primers from https://www.genewiz.com.cn	CaN is cloned from adult zebrafish fin cDNA library
transfected construct (human)	CMV-Kirin	Shen	Shen et al., 2019	
biological sample (zebrafish)	Adult zebrafish fin tissue	this paper	this paper	Freshly isolated after heatshock at indicated time points
antibody	Anti-GFP (mouse monoclonal)	Invitrogen	Cat. #: MA5-15349 RRID:987186	IF(1：400)
antibody	Anti-β-catenin (rabbit polyclonal)	Cell Signaling	Cat. #: 9562L RRID:B_331149	WB(1:1000) IF(1:400)
Antibody	Anti-Lef1(rabbit monoclonal)	Cell Signaling	Cat. #:2230T RRID:AB_823558	WB (1:1000)

antibody	Anti-Shh(rabbit polyclonal)	Novus	Cat. #: NBP2-22139	WB (1:1000)
antibody	Anti-mCherry antibody(rabbit polyclonal)	Invitrogen	Cat.#:PA534974 RRID :AB_2552323	IF(1:1000)
antibody	Anti-mouse-GFP (goat polyclonal)	Abcam	Cat.#:ab150113 RRID:AB_2576208	IF(1:1000)
antibody	goat-anti-rabbit-mCherry secondary antibody(Goat polyclonal)	Abcam	Cat.#:ab150078 RRID:AB_2722519	IF(1:2000)
antibody	Anti-Mouse IgG (goat Polyclonal)	Sigma	Cat. #:A3682-1ML RRID:AB_258100	WB(1:80000)
antibody	Anti-Rabbit IgG (H+L) (donkey Polyclonal)	Jackson	Cat. #:711-036-152 RRID:AB_2340590	WB(1:20000)
antibody	Anti-β-Actin pAb-HRP-DirecT (rabbit Polyclonal)	MBL	Cat. #:PM053-7 RRID:AB_10697035	WB(1:2000)

antibody	Anti-Digoxigenin-AP, Fab fragments(sheep polyclonal)	Roche	Cat.#:11093274910	Insitu(1:5000)
recombinant DNA reagent	NovoRec® plus One step PCR Cloning Kit	novoprotein	Cat. #:NR005-01B	
sequence-based reagent	F-kcnk9	this paper	Pcr primers	ATGAAGAGGCAGAACGTGCGGACGC
sequence-based reagent	R-kcnk9	this paper	Pcr primers	GATGGACTTGCGTCGTCTCATAAGCCGG
sequence-based reagent	F-kcnk10	this paper	Pcr primers	ATGAAATTTCCAACGGAAAACCCGAGGAAG
sequence-based reagent	R-kcnk10	this paper	Pcr primers	CTATGGATCCACCTGCAAACGGAACTC
commercial assay or kit	Protein Quantitative Kit (BCA)	MDBio	Cat. #:KT054-200rxn	
chemical compound, drug	FK506	Sigma	Cat. #:F4679-5MG	
chemical compound, drug	DL-Dithiothreitol	Promega	Cat. #:P117B	

chemical compound, drug	Adenosine 5'-triphosphate disodium salt hydrate	sigma	Cat. #:A2383	
chemical compound, drug	Nitro Blue Tetrazolium	Sigma	Cat. #:N6639	
chemical compound, drug	BCIP	sigma	Cat. #:B-8503	
chemical compound, drug	DAPI	Roche	Cat.#:10236276001	
software, algorithm	ImageJ	Open source	RRID:SCR_003070	https://imagej.nih.gov/ij/
software, algorithm	SymPhoTime 64	PicoQuant	RRID:SCR_016263	Used to analysis flim data
software, algorithm	Zen Blue	Zeiss	RRID:SCR_013672	
software, algorithm	Patchmaster	Heka	RRID:SCR_000034	
software, algorithm	Graphpad prism	Graphpad Software	RRID:SCR_002798	
software, algorithm	Clampfit10.5	Axon	RRID:SCR_011323	
other	Express Plus PAGE	Genscript	Cat.#:M81615C	For western blotting

	Gel, 8-16%, 15 wells			
other	Western Lightning Plus ECL 680	PerkinElmer(PE)	Cat.#:NEL105001EA	For western blotting
other	MMESSAGE MMACHINE SP6 KIT	Invitrogen	Cat.#:AM1340	

Cloning

Constructs were designed either using standard restriction enzyme or by homologous recombination methods. *kcnk5b* cDNA was isolated by RT-PCR from regenerating adult fin cDNA library and cloned into MCS region of pcDNA6-myc-6xHIS-tag plasmid (Invitrogen) or pBluescript harboring the *hsp70* zebrafish promoter and GFP coding sequence surrounded by 2 miniTol2 sites. Mutagenesis of the Serine345 codon of Kcnk5b was performed using QuikChange Mutagenesis kit (Agilent).

Zebrafish Husbandry

AB strain fish were raised in 10L tanks with constantly flowing water, 26ºC standard light-dark cycle (Brand et al., 2002) in either a Schwarz (DFG-Center for Regeneration, TU Dresden) or HaiSheng aquarium (ShanghaiTech University) systems. Transgenic lines harboring the different *kcnk5b* transgenes were created by injecting 300 µg of each construct together with mRNA of Tol2 transposase (Balciunas et al., 2006). Fish harboring Tg[7*XTCF-Xla.sam*:mCherry] transgene are deposited in the European Zebrafish Resource Center. Fish embryos and larva were raised in 1xE3 medium (5mM NaCl, 0.17mM KCl, 0.33mM $CaCl_2$, 0.33mM $MgSO_4$, 10^{-5}% Methylene Blue) until 10-12dpf, then transferred to aquarium water tanks to grow. Transgenic lines established by screening for GFP expression after heat shock. Experiments used male and female fish equally. Fish experiments were compliant to the general animal welfare guidelines and protocols approved by legally authorized animal welfare committees (Technische Universität Dresden, Landesdirektion Dresden, and ShanghaiTech University, ShanghaiTech Animal Welfare Committee).

Heat-shock induction of transgenes

Parents of heat-shock-driven transgenic lines were either outcrossed to same-strain wild-type fish or to fish harboring Tg[*7XTCF-Xla.sam*:mCherry]transgene. Progeny were collected in 1xE3 and raised at 28^{0}C. Carriers were confirmed positive for their respective transgenes by a single heat shock at 37^{0}C for 1 hour. For embryo experiments, heat shock was at 12hpf or 32 hpf (pectoral fin bud) in 37ºC E3 medium for 30 min. For larva the heat shock was in 37ºC E3 medium for 30 min. at 2 dpf. For adult fin, 6 month-old fish underwent a daily heat-chock regimen: first, sedated in 0.04% tricane in aquarium water, then placed in conical tubes containing 0.04% tricane in aquarium water to allow continued gill movement in oxygenated water and allow the caudal fins to be exposed to 37ºC water for 7 min. After heat shocking the caudal fin, the fish were returned to flowing aquarium water and monitored daily. Caudal fin measurements were made from the base of the fin to the distal tip along the third fin ray of each fin lobe counting in from the dorsal-most and ventral-most sides. Body lengths were determined by measuring the most anterior point of the jaw to the base of the caudal fin. Larval finfold measurements were from the ventral-most to dorsal-most points of the caudal finfold or from the anterior-most to the posterior-most points of the ventral finfold along the body length. Body lengths of larva were measured from the anterior-most point of the jaw to the posterior-most point of the somatic musculature.

Western Blotting

Fins were amputated and snap frozen in liquid nitrogen and homogenized in RIPA buffer (Proteintech, B100020) with protease inhibitor (Pierce, 88666) and then rotated at 4℃ for 2h to lysate cells thoroughly. Protein was collected and concentration was quantified by BCA assay (MDBio, KT054-200rxn) after centrifuge at 12000rpm at 4℃ for 20min. Then gel electrophoresis was conducted at 120V for 90min using page gels (Genscript, M81615C), protein were then transferred to PVDF membranes (Bio-Rad, 1620177). Anti-lef1 (1:1000, Cell Signaling Technology, 2230T, RRID: AB_823558)), Anti-shh (1:1000, Novus, NBP2-22139, RRID: AB_331149), Anti-β-catenin (1:1000, Cell Signaling Technology, 9562L), Anti-β-Actin pAb-HRP-DirecT (1:2000, MBL, PM053-7, RRID: AB_10697035) were used as primary antibodies to incubate overnight at 4℃. Anti-Rabbit IgG (1:20000, Jackson, 711-036-152, RRID: AB_2340590) were used as secondary antibody and blots were detected using ECL detection (PerkinElmer (PE), NEL105001EA), and Image J software (RRID: SCR_003070) was used for density quantification.

In situ hybridization

mRNA probes were made from RT-PCR products isolated from 2 dpf zebrafish embryos 6 hours after 37.5°C heat shock. The primer sequences for generating the probes are F- *shha*:5'-TGCGGCTTTTGACGAGAGTGC-3'R-shha: 5'-GGTAATACGACTCACTATAGGG TTTCCCGCGCTGTCTGCCG-3' F-lef1 : 5'-GAGTTGGACAGATGACCCCTCCTC-3'; R-lef1：5'-GGTAATACGACTCA CTATAGGGGCAGACCATCCTGGGTAAAG-3'. *in vitro* transcription reagents are from Promega. Isolated fish fins were surgically isolated and incubated in 4% PFA in 1xPBS at 4ºC overnight with gentle rocking. Samples were subsequently washed 5 times in 1xPBS and then dehydrated by incubation for 15 min in a graded series of increasing methanol/1xPBS solutions (25%, 50%, 75%, 3x 100%) on ice. Fins were then incubated in 100% methanol for ⩾2hrs at -20ºC. Samples were then rehydrated using the reversed dehydration series of methanol/1xPBS solutions). Samples were then incubated more than 4x in 1xPBS to remove all methanol, and subsequently incubated in 10µM Proteinase K for 10 min at RT. Samples were then incubated 20 min. in 4% PFA/1xPBS to inactivate the Proteinase K. Samples were incubated in 1xPBS 6x 10 mins to remove the PFA, then incubated in pre-hybridization buffer for 2 hours at 65C. Samples were subsequently incubated in the hybridization solution containing 200ng/ml of each mRNA probe ⩾ 14 hrs at 65ºC. Samples then were washed with successive wash steps to remove unbound probe and prepare for antibody incubation: twice 2xSSC/50% deionized formalin at 65ºC, twice 2xSSC/25% deionized formalin at 65ºC, 2xSSC at 65ºC, twice 0.2xSSC at RT, 6 times 1xPBST (1xPBS with Tween-20), once in blocking solution [2% Bovine albumin (Sigma-Aldrich, A3294-100G), 2% Sheep Serum (Meilunbio, M134510)] at RT for 4 hours. Samples were incubated with Anti-digoxigenin-AP Fab Fragment (Sigma-Aldrich, 11093274910, RRID: AB_514497) in blocking solution ⩾14 hrs at 4ºC. Samples were then washed 6 times with 1xPBST, subsequently incubated in [0.1 M Tris-HCl, pH 9.5, 0.1 M NaCl, 0.05 M $MgCl_2$] 3 times for 30 min, and then in Nitro Blue Tetrazolium (Sigma-Aldrich, N6639-1G) and 5-bromo-4-chloro-3-indolyl phosphate (Sigma-Aldrich, 136149) in [0.1 M Tris-HCl, pH 9.5, 0.1 M NaCl, 0.05 M $MgCl_2$] at RT ⩾8hrs. Samples images under Stemi508 stereoscope (Zeiss) with Axiocam ERc5s digital color camera (Zeiss) and Zen2.3 software (Zeiss, RRID: SCR_013672). For signal areas and signal intensities analyses, images of the *shh in situs* were transferred to Fiji ImageJ (RRID SCR_003070). The stained regions were traced using "free ROI" and then quantitated using the

"measure" function under the "analysis" menu to calculate the number of pixels contained in the stained area. For signal intensity analysis, the signal region and adjacent unstained regions were measured by "free ROI" selection and the mean intensity pixel values were determined from the "measure" function under the analysis menu by subtracting the mean value of the unstained region from the mean value of the signal region for each fin bud.

Immunohistochemistry

Zebrafish fins or larvae euthanized in 1% Mesab were fixed in 4%PFA/1xPBS and embedded in 1% agarose (CryoStar NX50, Thermofisher) or tissue freezing medium (Leica, 14020108926) on dry ice. (CryoStar NX50, Thermofisher) before cryosectioning. 10 µm sections were mounted on glass slides (Titan, 02036398) and dried. The tissue freezing medium (Leica) was removed in ddH_2O for 10 min. Sections were permeabilized in 0.1%Triton-X for 5min and incubated in 1% BSA/1xPBS/0.1%Tween-20 (PBST) at room temperature for 30min. Sections were incubated in a mouse-anti-GFP (Invitrogen, MA5-15349, RRID:AB_10987186) solution (1:400), Anti-β-catenin (Cell Signaling, 9562L, RRID: AB_331149), Anti-Lef1 (Cell Signaling, 2230T, RRID: AB_823558) solution (1:1000), Anti-Shh (Novus, NBP2-22139, RRID: AB_2883969) solution (1:1000 dilution), rabbit-anti-mCherry antibody (Invitrogen, P5-34974, RRID: AB_2552323) solution (1:2000 dilution) in PBST at 4ºC overnight (>12 hours). The primary antibody solution was replaced by a goat-anti-mouse-GFP (Abcam, ab150113, RRID: AB_2576208), goat-anti-rabbit-mCherry secondary antibody (Abcam, ab150078, RRID: AB_2722519) solution (1:2000 dilution) in PBST and incubated at RT in the dark for 60 min. The secondary antibody solution was then replaced with DAPI solution (Roche, 10236276) in the dark at room temperature for 5 min. DAPI were washed away in 1xPBST 3x 5-min incubations at RT. Coverslips (Titan, 02036401) were mounted with a 40% glycerol solution and sealed with nail polish. The sections were visualized using an LSM710 upright scanning confocal (Zeiss) or a LSM880 inverted scanning confocal (Zeiss) with ZENBlue software (Zeiss, RRID: SCR_013672). Images were processed with Fiji software (RID: SCR_003070).

β-catenin nuclear analysis on IHC cross sections of fins

Using Fiji ImageJ, multiple nuclei of cells in IHC fin cross section image of control fins were manually measured, and a mean mRFP fluorescence intensity value was calculated. This mean value was used as the baseline for assessing nuclear β-catenin levels. β-catenin nuclear

values for all the nuclei in each cross section were assessed with ImageJ by splitting the combined images of β-catenin and DAPI and using DAPI to have Fiji ImageJ define and select all nuclei in the image. The nuclear β-catenin levels were determined in selected nuclei by intensity analysis in Fiji ImageJ (RID: SCR_003070), which provided a numeric value for the β-catenin channel in all the nuclei of each section.

Cell Transplantations

Transgenic fish lines [*hsp70*:*kcnk5b*-GFP] and [7XTCF-Xla.sam:mCherry] were inbred for 20-30 min before embryos were collected in E3. The genotypes of the parents and of the imaged progeny were confirmed to be homozygous for the 7XTCF-Xla.sam:mCherry transgene by qPCR . Primers for genomic β-actin locus were used as DNA content standardization. The cycle procedure was at 50.0°C for 2 min, 95.0°C for 10 min in the hold step; 95.0°C for 15 s, 55.0°C for 20s for 40 routine in the elongation step; 95.0°C for 15s, 60.0°C for 1 min, 95.0°C for 15s in the melting curve step. The embryos were left to develop in E3 for 3-3.5 hours at 28^{0}C until the blastula stage. Embryos were then placed in agarose ridges for easy access under a Zeiss stereomicroscope and cells from the [*hsp70*:*kcnk5b*-GFP] embryos were isolated by air suction via a glass needle mounted on a Precision Instruments piston. The [*hsp70*:*kcnk5b*-GFP] cells were then transplanted into the [*7XTCF-Xla.sam*:mCherry] embryos. The transplants were carefully moved from the agarose into clean 90mm dishes with fresh E3 (+/- 20-25 per dish) and incubated at 28^{0}C. One or two days after transplantation, fish were heat shocked for 1 hour at 37^{0}C. Four hours after heat shock, 48- or 72-hour fish were embedded into 1% low melting agarose (Sigma-Aldrich-Aldrich, A9414-250G) supplemented with Mesab in 35mm glass bottom confocal dishes (Cellvis: D35-20-1-N) and turned to their side. Visualized with a LSM710 confocal argon laser microscope (Zeiss) with ZENBlue software (Zeiss, RRID: SCR_013672).

qRT-PCR

The cDNA that was used for qRT-PCR was extracted from the HEK293T cells and zebrafish. The mRNA was isolated using Tri-Reagent (CWBio, 03917). Then 1μg mRNA was used for the reverse transcription to cDNA using 4x gDNA wiper Mix, 5x HiScript III qRT SuperMix (Vazyme, L/N 7E350C9). qRT-PCR was performed using 2x ChamQ Universal SYBR qPCR Master Mix (Vazyme, L/N TE342F9) with QuantStudio3 machine (Thermofisher). The cycle procedure was at 50.0°C for 2 min, 95.0°C for 10 min in the stage 1; 95.0°C for 15 s, 60.0°C for

20s for 40 routine in the stage2; 95.0ºC for 15s, 60.0ºC for 1 min, 95.0ºC for 15s in the Melt Curve. Samples were standardized using the detected β-actin expression for fish mRNA isolation and GAPDH for human cell line mRNA isolations. The data was analyzed in the ΔΔCt method.

Cell Culture

All cell culture lines were incubated at 37ºC, 5% CO2, 95% humidity in incubators (Thermofisher, FORMA STERI-CYCLE i160) in DMEM medium (Gibco,1199506) with 10% FBS (Gibco,1009914) and 1% penicillin streptomycin (Gibco, 15140122). The identity of the cell lines was not authenticated, and mycoplasma was not determined. Cell were split to 50% density and transfected with Lipofectamine™ (Invitrogen, 11668-019) 12 hours later. Expression for the transfected constructs was evaluated by expression of fluorescent marker.

Mycoplasma test

2 μ l of DMEM medium from different cultured cells are freshly taken as template. Primers to detect mycoplasma are used as F : 5'-GGGAGCAAACAGGATTAGATACCCT-3'; R：5'-TGCACCATCTGTCACTCTGTTAACCTC-3', then standard PCR was conducted (TOYOBO, KOD-401). The procedure is: Step1: 98 ºC for 2min. Step2: 98 ºC for 10s, 55 ºC for 30s, and 68 ºC for 30s for 30cycles. Step3:68 ºC for 10min, 4 ºC to hold. Then gel electrophoresis was conducted at 120v for 30min.

FRET-FLIM detection and analysis

Hek293T cells were transfected with 1μg of pcDNA-*kcnk5b*-GFP and 1μg of the pcDNA6-Kirin-FRET sensor (Shen et al., 2019). Fluorescence lifetime imaging measurements were made by photon counting the fluorescence emission of CFP using a 2-photon-confocal Hyperscope (Scientifica, UK) and PMT-hybrid 40 MOD 5 photon detectors (Picoquant, Germany). Counted photon emissions were calculated and analyzed using SymPhoTime 64, version 2.4 (Picoquant, Germany, RRID: SCR_016263).

Electrophysiology

Transfected HEK293T cells were seeded on glass coverslips (Fisher Brand), and incubated in cell culture medium at 37ºC, 5% CO_2, 95% relative humidity for 4-6 hours. The seeded coverslips were transferred into Tyrode's solution (138 mM NaCl, 4 mM KCl, 2 mM $CaCl_2$,1 mM $MgCl_2$, 0.33 mM NaH_2PO_4, 10 mM Glucose, 10 mM HEPES). Cells were assessed in the ruptured-patch whole-cell configuration of the patch-clamp technique using and EPC9 or EPC10 amplifier (HEKA) with borosilicate glass pipettes (Sutter Instruments) with 3-6 MΩ resistance when filled with pipette solution (130 mM glutamic acid, 10 mM KCl, 4 mM MgCl2, 10 mM HEPES, 2 mM ATP, pH to 7.2). After gigaseal formation, cells were voltage-clamped at -80 mV. Potassium conductance was elicited by test pulses from -100 mV to 70 mV (in 10mV increments) of 600 ms duration at a cycle length of 10s. The resulting tracings were converted into itx files by the ABF Software (ABF Software, Inc., RRID: SCR_019222) and then analyzed using Clampfit™ Software (Molecular Devices, RRID: SCR_011323). Currents were measured at the end of the test pulses.

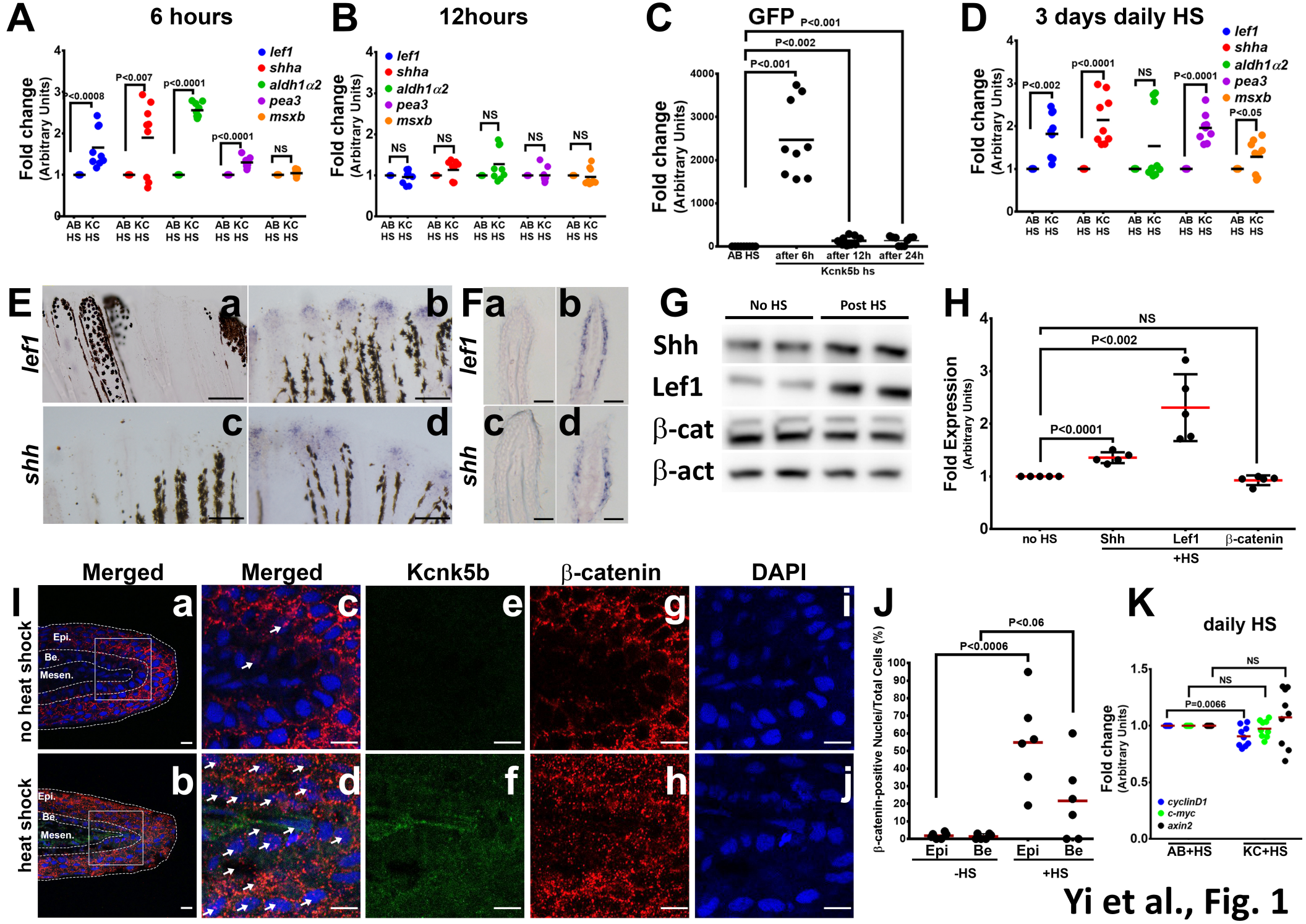
A
6 hours
Fold change (Arbitrary Units)
lef1
shha
aldh1α2
pea3
msxb
<0.0008
P<0.007
p<0.0001
p<0.0001
NS
AB HS
KC HS
B
12hours
NS
NS
NS
NS
NS
C
GFP P<0.001
P<0.002
P<0.001
AB HS
after 6h
after 12h
after 24h
Kcnk5b hs
D
3 days daily HS
P<0.002
p<0.0001
NS
P<0.0001
P<0.05
E
lef1
shh
a
b
c
d
F
a
b
c
d
G
No HS
Post HS
Shh
Lef1
β-cat
β-act
H
Fold Expression (Arbitrary Units)
NS
P<0.002
P<0.0001
no HS
Shh
Lef1
β-catenin
+HS
I
Merged
Merged
Kcnk5b
β-catenin
DAPI
no heat shock
heat shock
Epi.
Be.
Mesen.
J
β-catenin-positive Nuclei/Total Cells (%)
P<0.06
P<0.0006
Epi
Be
Epi
Be
-HS
+HS
K
daily HS
Fold change (Arbitrary Units)
NS
NS
P=0.0066
cyclinD1
c-myc
axin2
AB+HS
KC+HS
Yi et al., Fig. 1

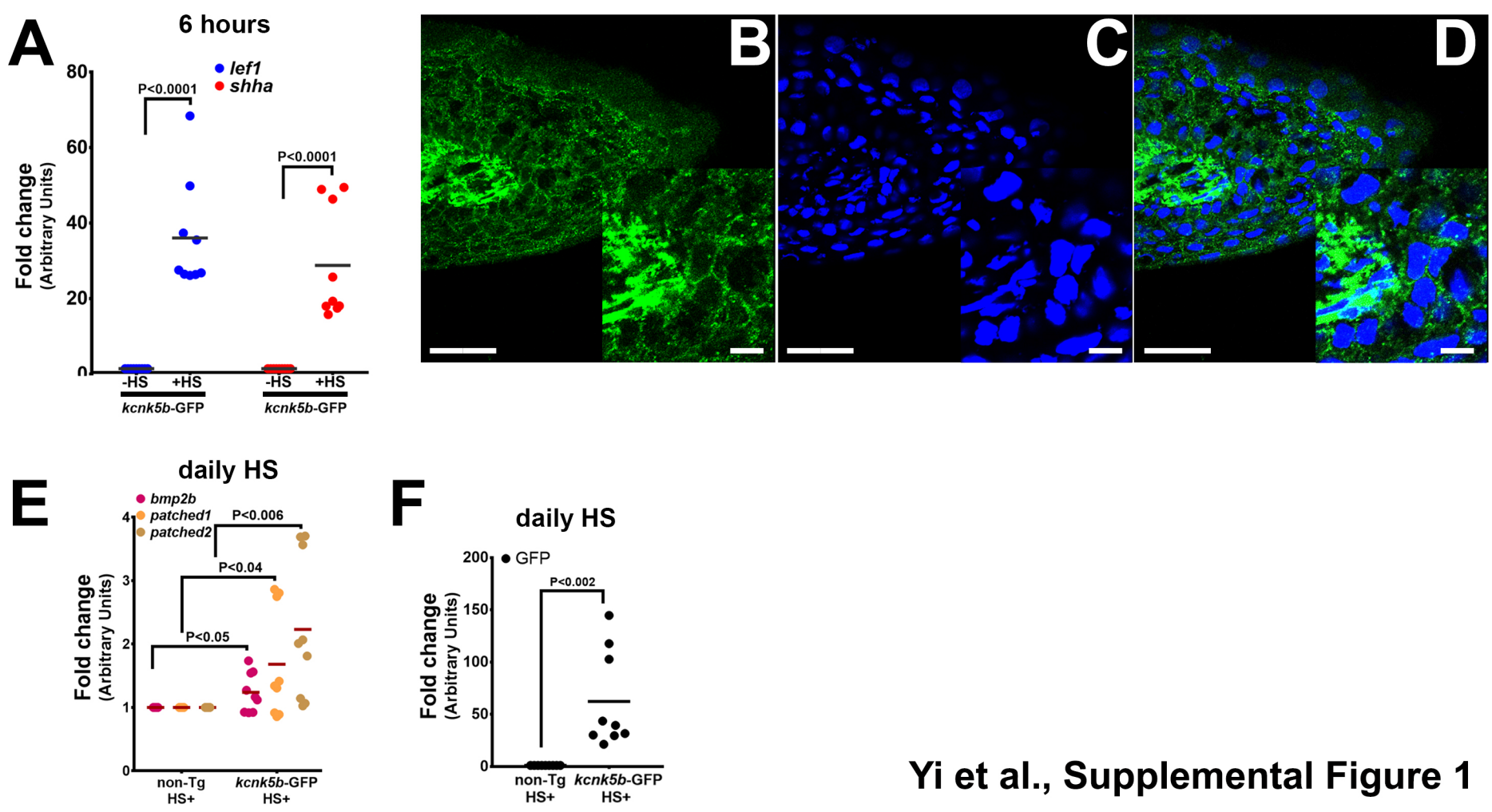

Yi et al., Supplemental Figure 1

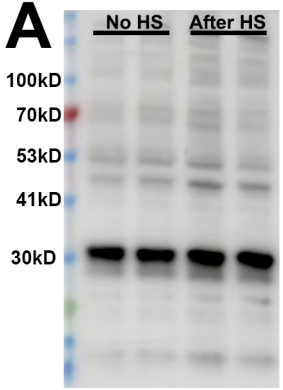

Shh

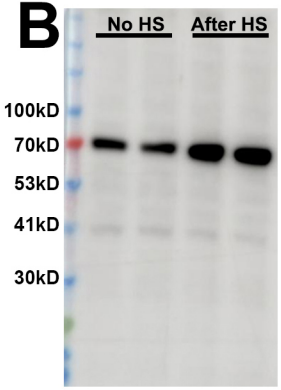

Lef1

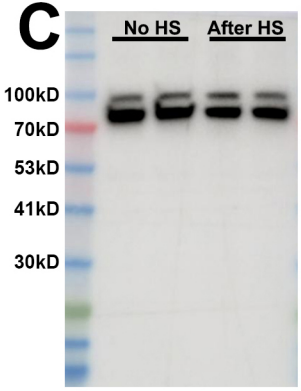

β-catenin

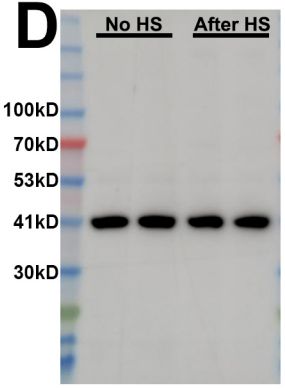

β-actin

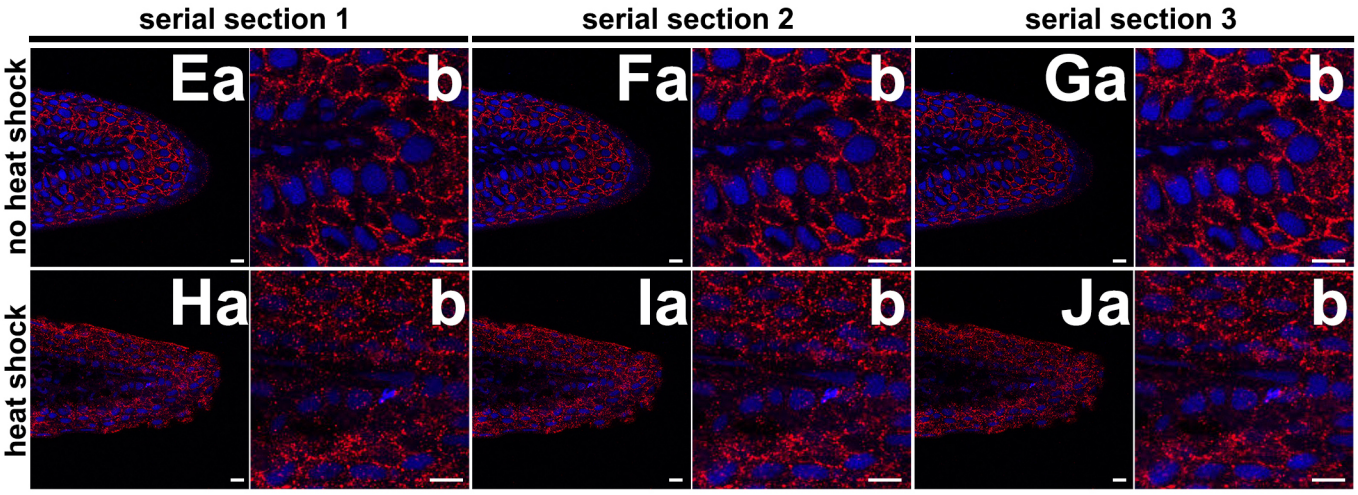

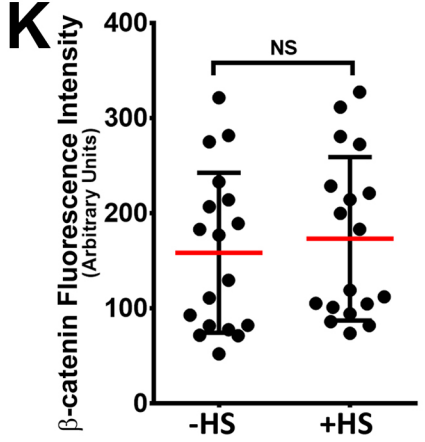

Yi et al., Fig. 1-Suppl. Fig. 2

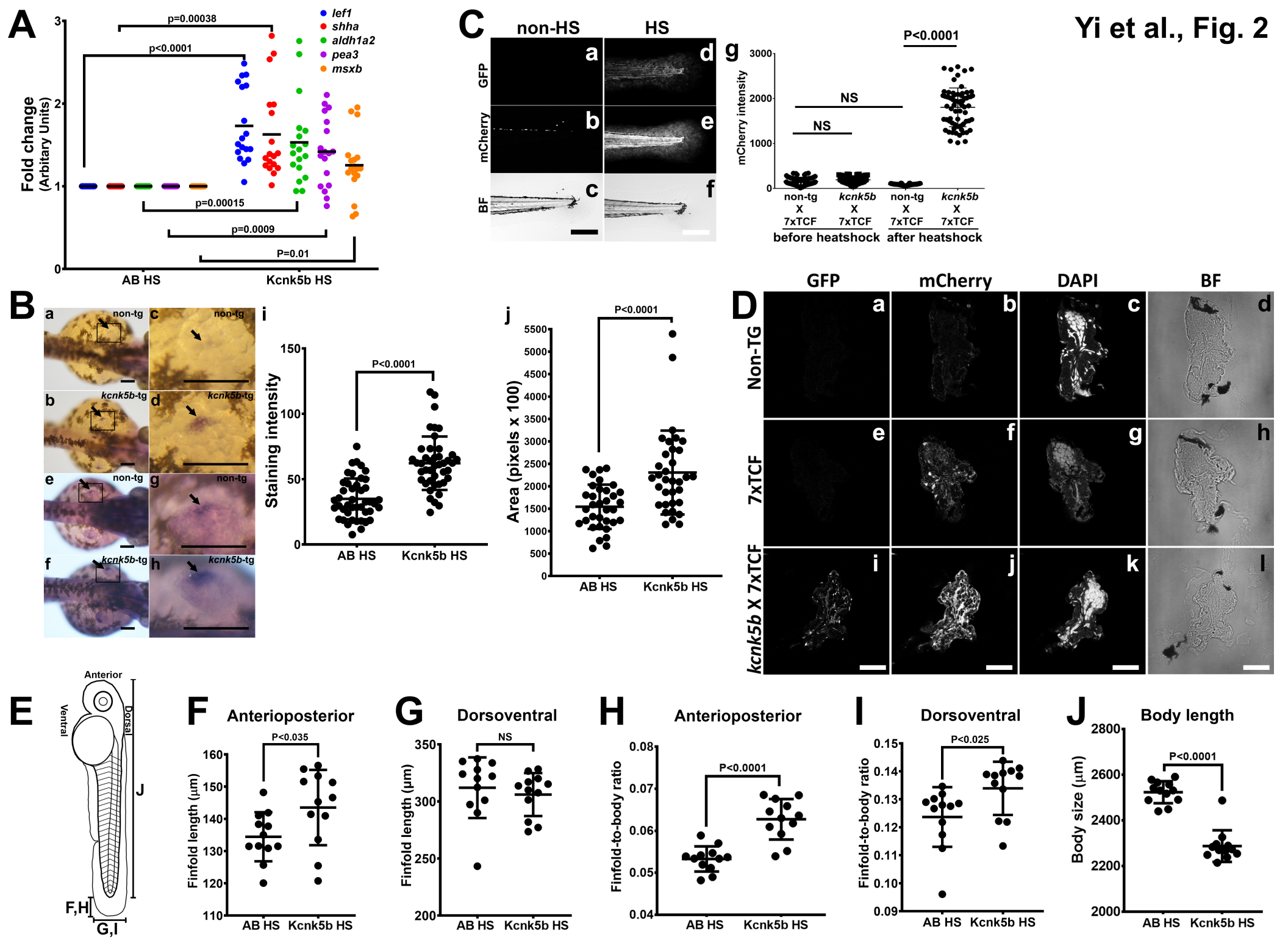
Yi et al., Fig. 2
A
lef1
shha
aldh1a2
pea3
msxb
Fold change (Arbitary Units)
p=0.00038
p<0.0001
p=0.00015
p=0.0009
P=0.01
AB HS
Kcnk5b HS
B
non-tg
kcnk5b-tg
i
Staining intensity
P<0.0001
AB HS
Kcnk5b HS
j
Area (pixels x 100)
P<0.0001
AB HS
Kcnk5b HS
C
non-HS
HS
GFP
mCherry
BF
g
mCherry intensity
P<0.0001
NS
NS
non-tg X 7xTCF
kcnk5b X 7xTCF
non-tg X 7xTCF
kcnk5b X 7xTCF
before heatshock
after heatshock
D
GFP
mCherry
DAPI
BF
Non-TG
7xTCF
kcnk5b X 7xTCF
E
Anterior
Ventral
Dorsal
J
F,H
G,I
F
Anterioposterior
P<0.035
Finfold length (µm)
AB HS
Kcnk5b HS
G
Dorsoventral
NS
Finfold length (µm)
AB HS
Kcnk5b HS
H
Anterioposterior
P<0.0001
Finfold-to-body ratio
AB HS
Kcnk5b HS
I
Dorsoventral
P<0.025
Finfold-to-body ratio
AB HS
Kcnk5b HS
J
Body length
P<0.0001
Body size (µm)
AB HS
Kcnk5b HS

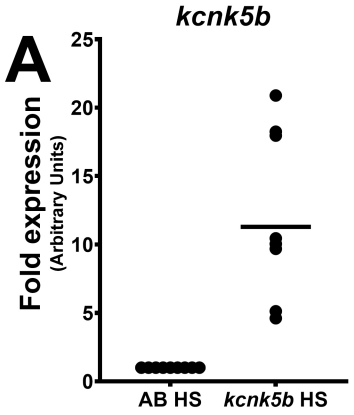

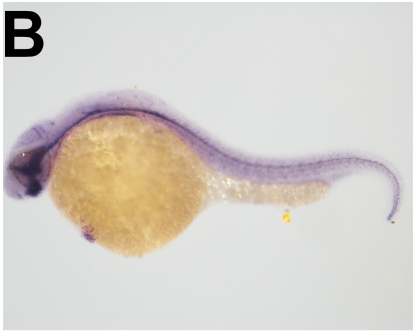

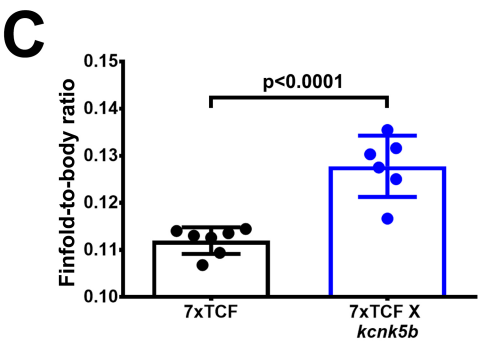

Yi et al., Fig. 2-Suppl. Fig. 1

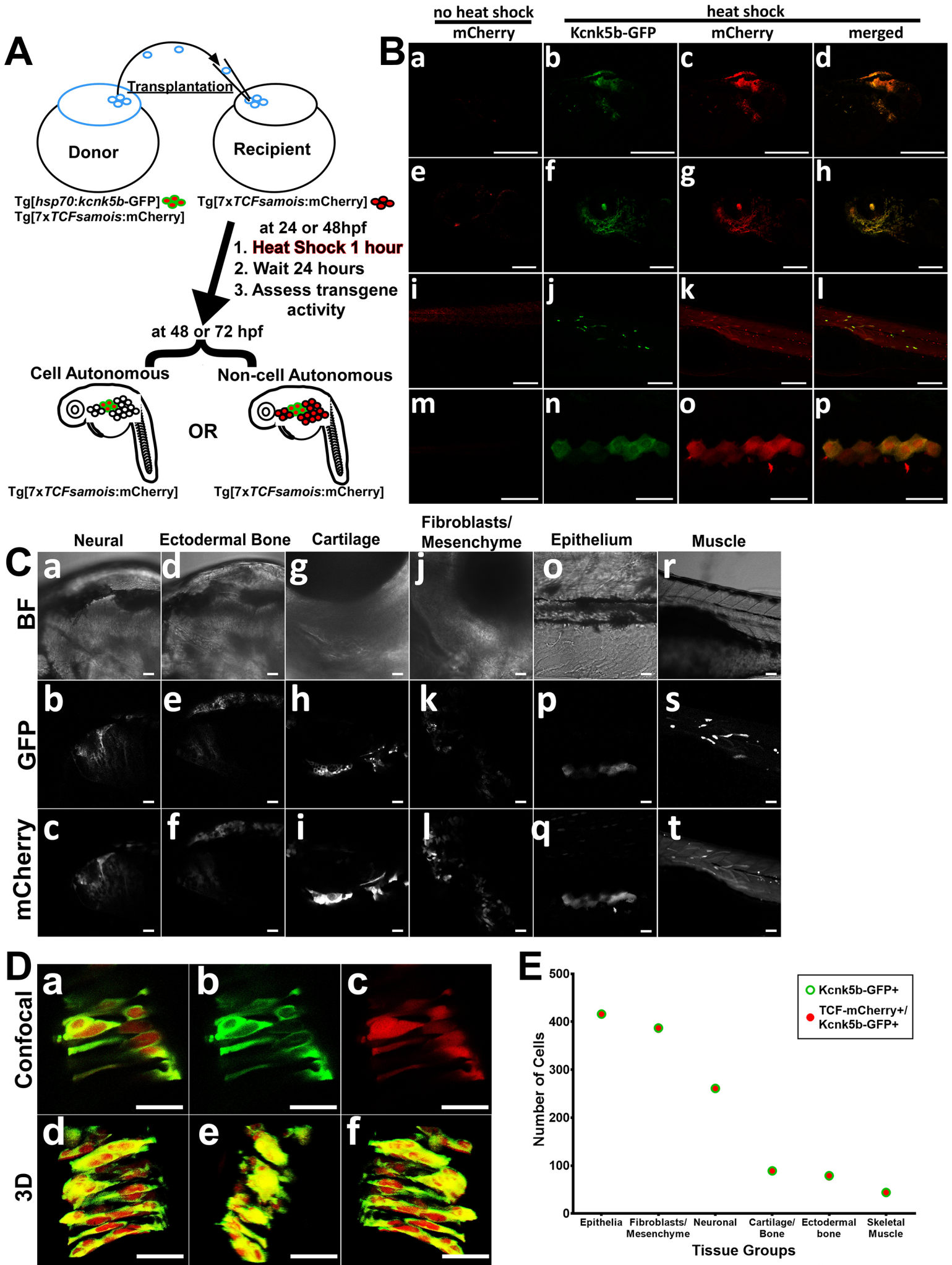
A
Transplantation
Donor
Recipient
Tg[hsp70:kcnk5b-GFP]
Tg[7xTCFsamois:mCherry]
Tg[7xTCFsamois:mCherry]
at 24 or 48hpf
1. Heat Shock 1 hour
2. Wait 24 hours
3. Assess transgene activity
at 48 or 72 hpf
Cell Autonomous
Non-cell Autonomous
OR
Tg[7xTCFsamois:mCherry]
Tg[7xTCFsamois:mCherry]
B
no heat shock
heat shock
mCherry
Kcnk5b-GFP
mCherry
merged
C
Neural
Ectodermal Bone
Cartilage
Fibroblasts/ Mesenchyme
Epithelium
Muscle
BF
GFP
mCherry
D
Confocal
3D
E
Number of Cells
Kcnk5b-GFP+
TCF-mCherry+/ Kcnk5b-GFP+
Epithelia
Fibroblasts/ Mesenchyme
Neuronal
Cartilage/ Bone
Ectodermal bone
Skeletal Muscle
Tissue Groups

Yi et al., Fig. 3

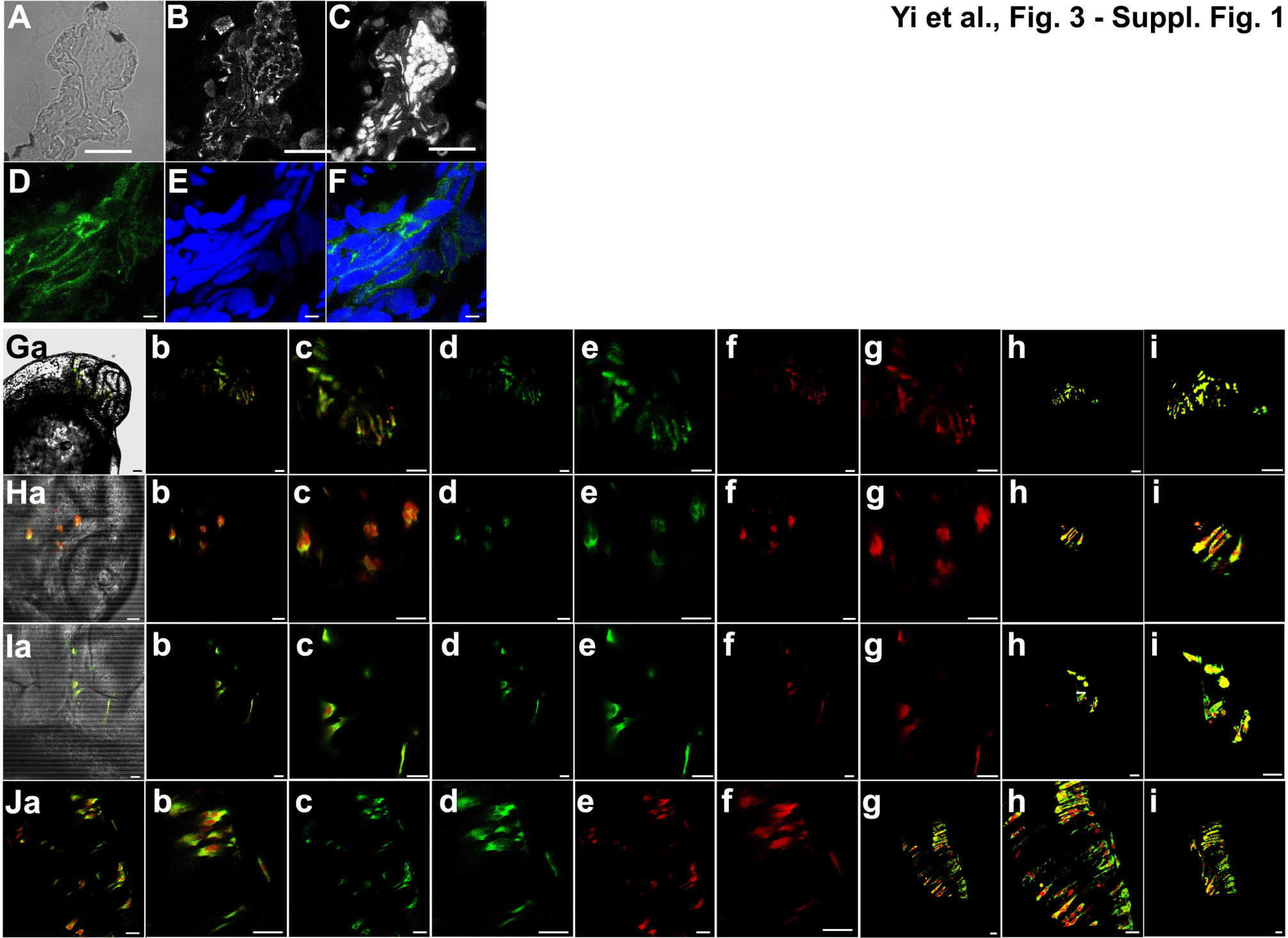
A
B
C
D
E
F
Ga
Ha
Ia
Ja
b
c
d
e
f
g
h
i

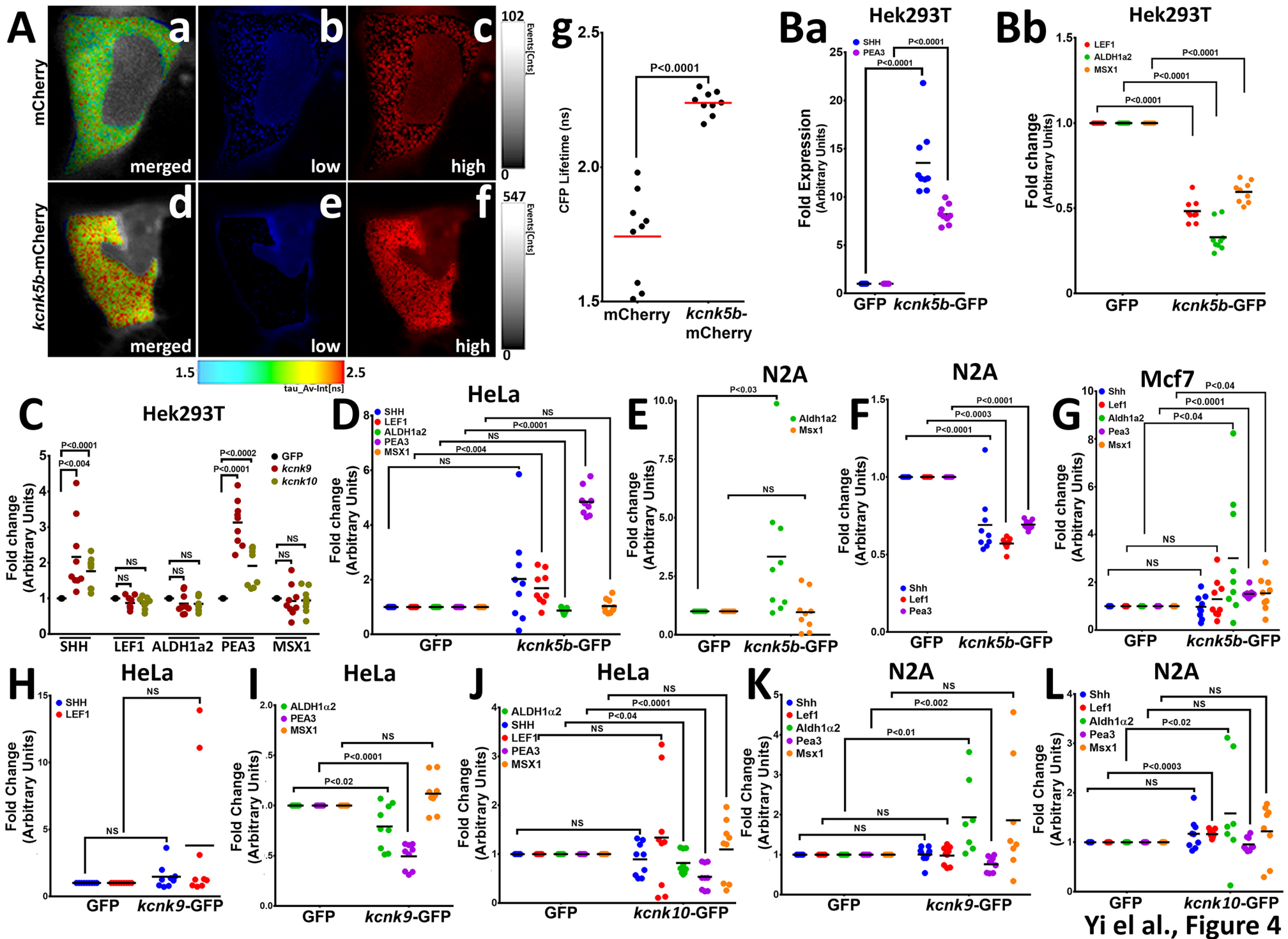
A
a
b
c
d
e
f
mCherry
kcnk5b-mCherry
merged
low
high
merged
low
high
102
0
547
0
Events[Cnts]
Events[Cnts]
1.5
2.5
tau_Av-Int[ns]
g
CFP Lifetime (ns)
P<0.0001
mCherry
kcnk5b-mCherry
Ba
Hek293T
SHH
PEA3
P<0.0001
P<0.0001
Fold Expression
(Arbitrary Units)
GFP
kcnk5b-GFP
Bb
Hek293T
LEF1
ALDH1a2
MSX1
P<0.0001
P<0.0001
P<0.0001
Fold change
(Arbitrary Units)
GFP
kcnk5b-GFP
C
Hek293T
P<0.0001
P<0.004
P<0.0002
P<0.0001
GFP
kcnk9
kcnk10
NS
Fold change
(Arbitrary Units)
SHH
LEF1
ALDH1a2
PEA3
MSX1
D
HeLa
SHH
LEF1
ALDH1a2
PEA3
MSX1
NS
P<0.0001
NS
P<0.004
NS
Fold change
(Arbitrary Units)
GFP
kcnk5b-GFP
E
N2A
P<0.03
Aldh1a2
Msx1
NS
Fold change
(Arbitrary Units)
GFP
kcnk5b-GFP
F
N2A
P<0.0001
P<0.0003
P<0.0001
Shh
Lef1
Pea3
Fold change
(Arbitrary Units)
GFP
kcnk5b-GFP
G
Mcf7
Shh
Lef1
Aldh1a2
Pea3
Msx1
P<0.04
P<0.0001
P<0.04
NS
NS
Fold change
(Arbitrary Units)
GFP
kcnk5b-GFP
H
HeLa
SHH
LEF1
NS
NS
Fold Change
(Arbitrary Units)
GFP
kcnk9-GFP
I
HeLa
ALDH1α2
PEA3
MSX1
NS
P<0.0001
P<0.02
Fold Change
(Arbitrary Units)
GFP
kcnk9-GFP
J
HeLa
ALDH1α2
SHH
LEF1
PEA3
MSX1
NS
P<0.0001
P<0.04
NS
NS
Fold Change
(Arbitrary Units)
GFP
kcnk10-GFP
K
N2A
Shh
Lef1
Aldh1α2
Pea3
Msx1
NS
P<0.002
P<0.01
NS
NS
Fold Change
(Arbitrary Units)
GFP
kcnk9-GFP
L
N2A
Shh
Lef1
Aldh1α2
Pea3
Msx1
NS
NS
P<0.02
P<0.0003
NS
Fold Change
(Arbitrary Units)
GFP
kcnk10-GFP
Yi el al., Figure 4

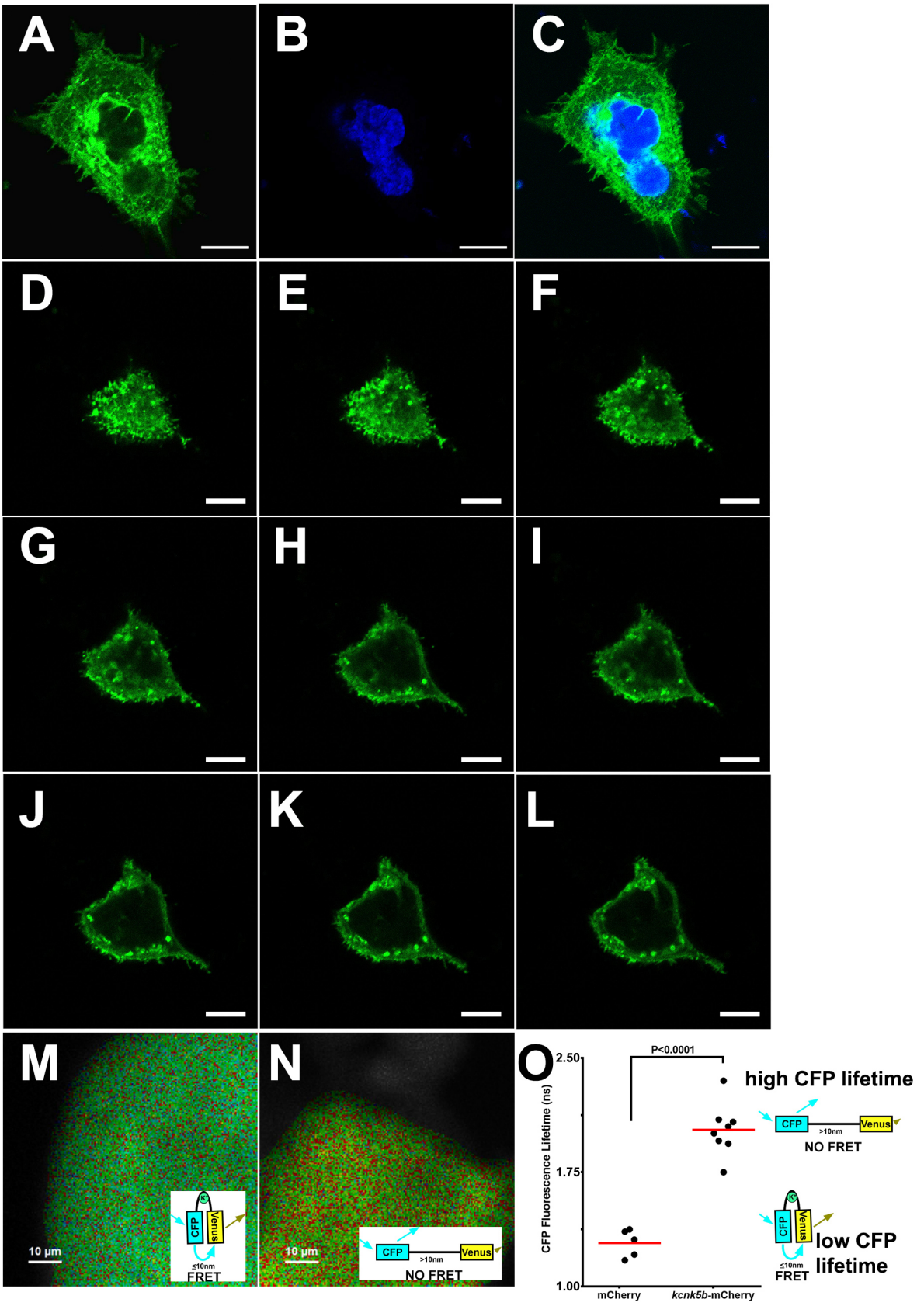

Yi et al., Fig. 4- Suppl. Fig. 1

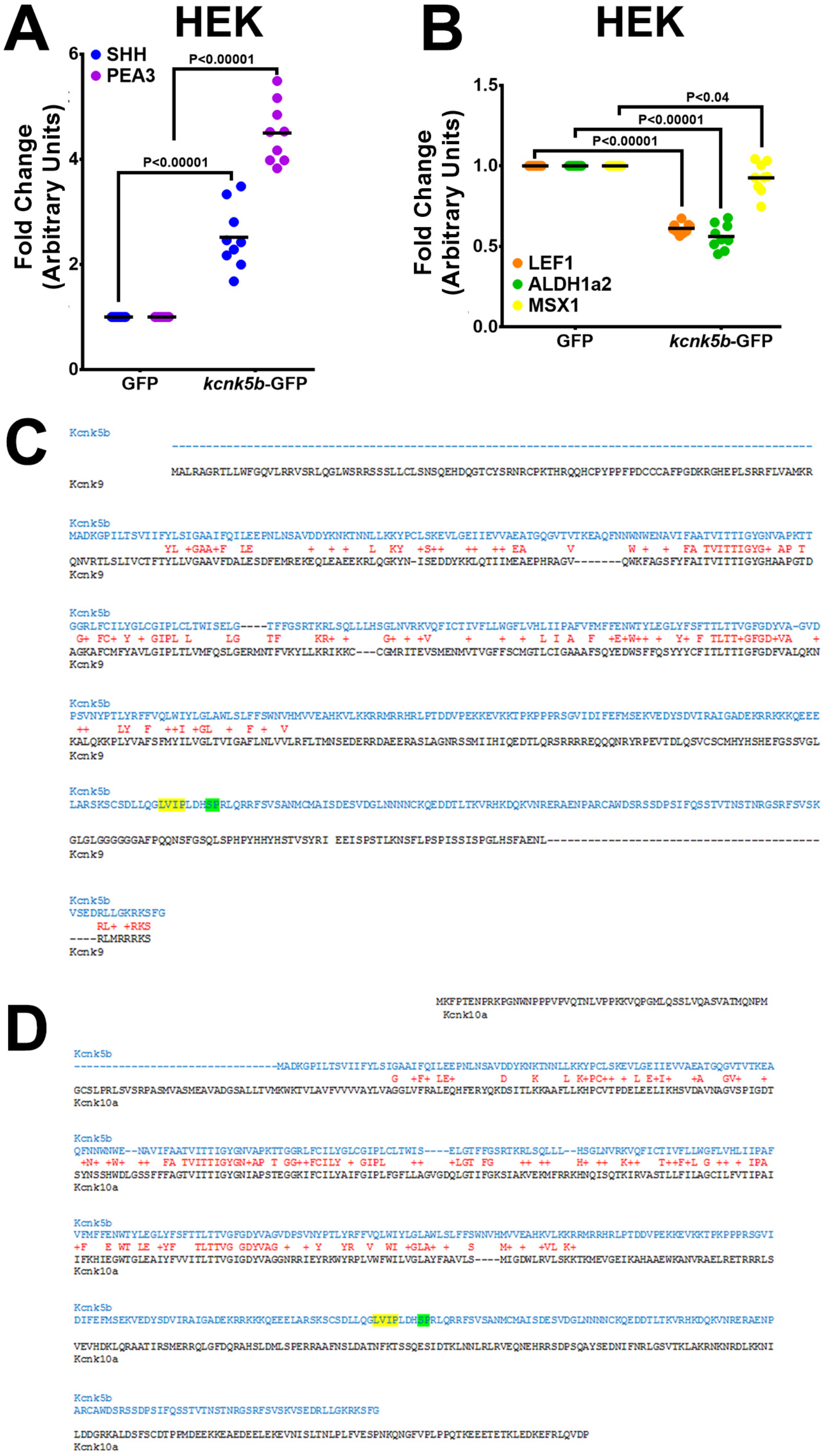

Yi et al., Fig. 4-Suppl. Fig. 2

Yi et al., Figure 5

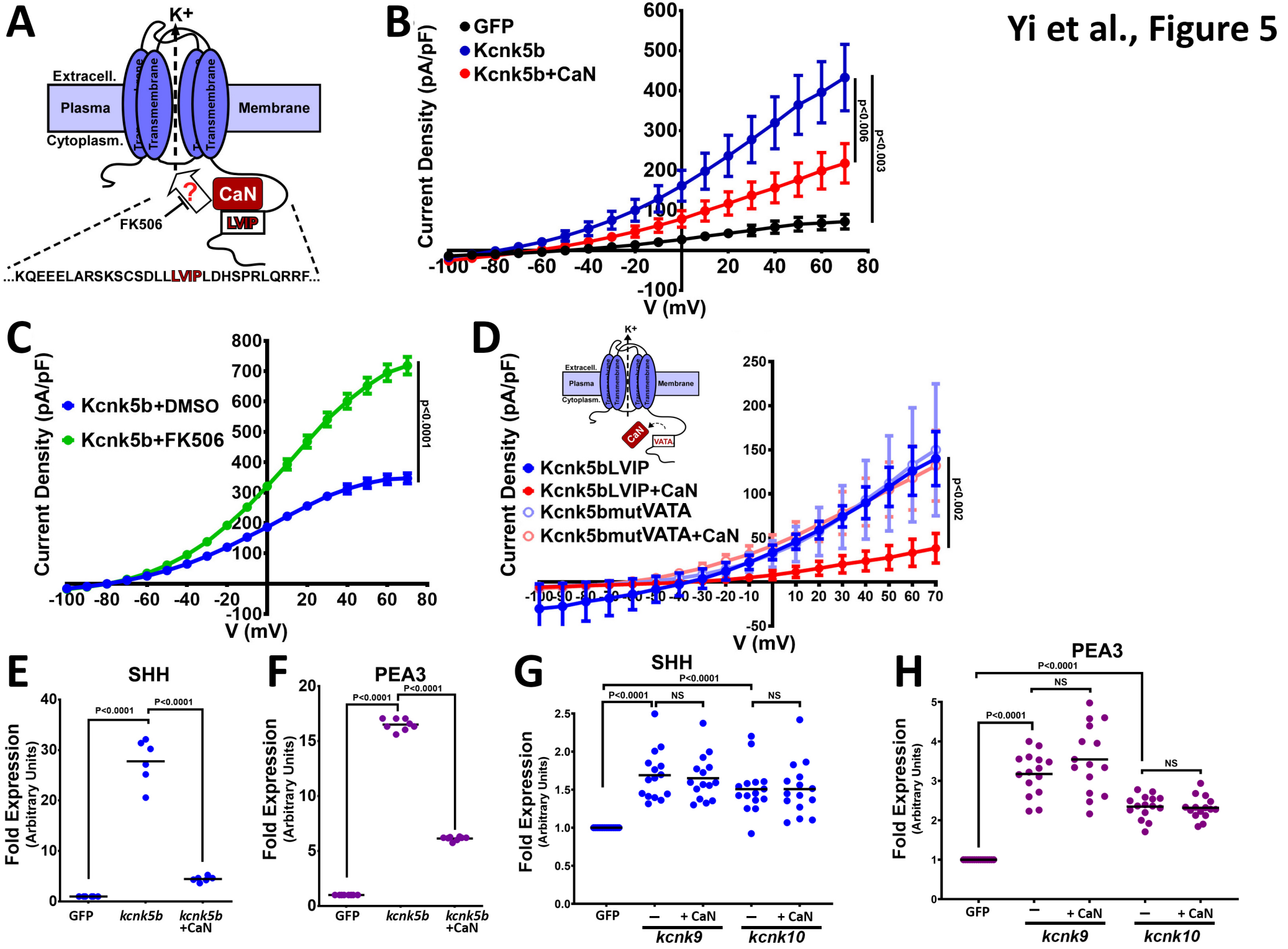

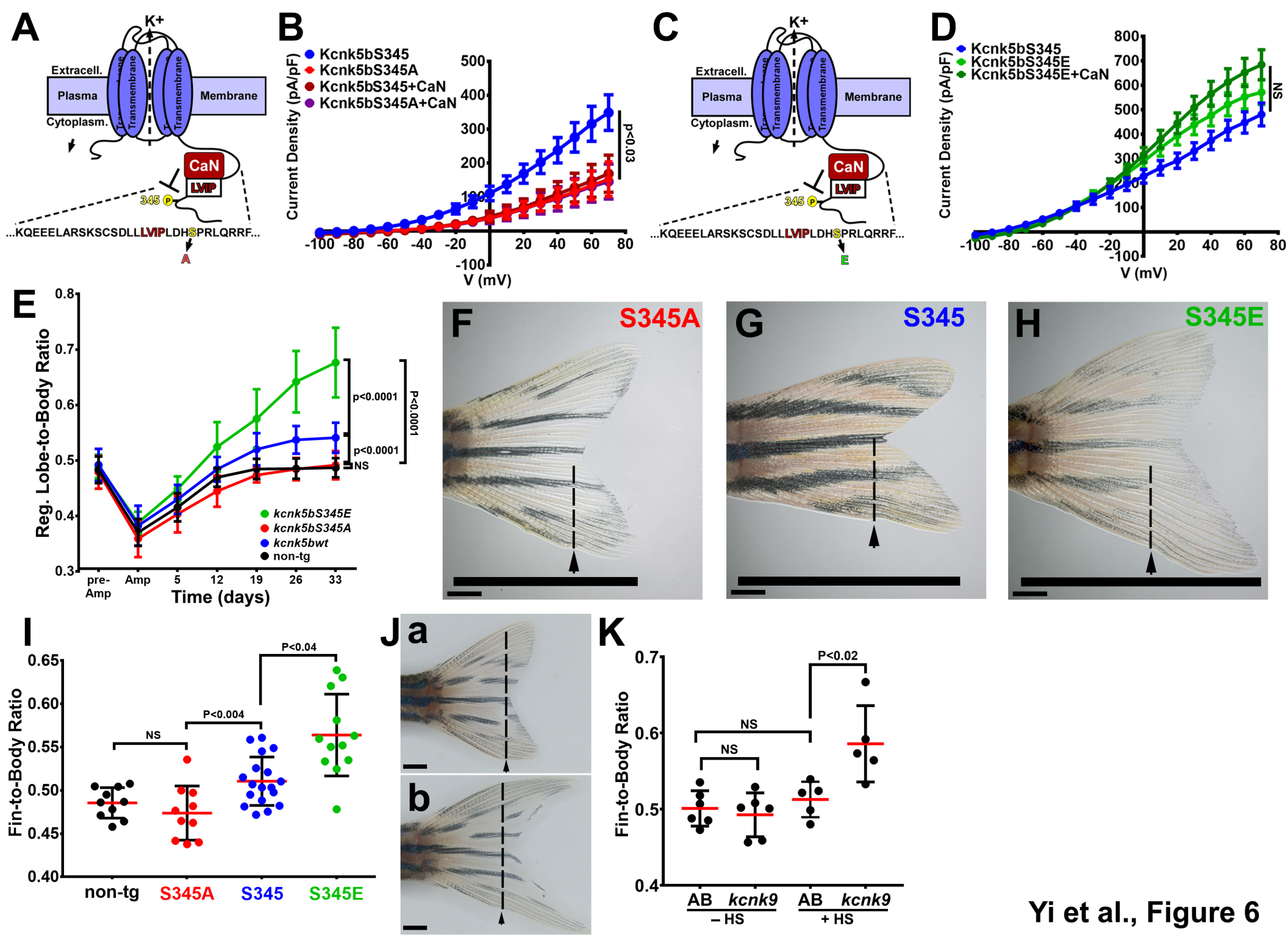
A
K+
Extracell.
Plasma
Membrane
Cytoplasm.
Transmembrane
CaN
LVIP
345
P
...KQEEELARSKSCSDLLLVIPLDHSPRLQRRF...
A
B
Kcnk5bS345
Kcnk5bS345A
Kcnk5bS345+CaN
Kcnk5bS345A+CaN
Current Density (pA/pF)
V (mV)
p<0.03
C
E
D
Kcnk5bS345E
Kcnk5bS345E+CaN
NS
E
Reg. Lobe-to-Body Ratio
Time (days)
pre-Amp
Amp
kcnk5bS345E
kcnk5bS345A
kcnk5bwt
non-tg
p<0.0001
P<0.0001
NS
F
S345A
G
S345
H
S345E
I
Fin-to-Body Ratio
P<0.04
P<0.004
NS
non-tg
S345A
S345
S345E
J
a
b
K
P<0.02
NS
AB
kcnk9
– HS
+ HS
Yi et al., Figure 6

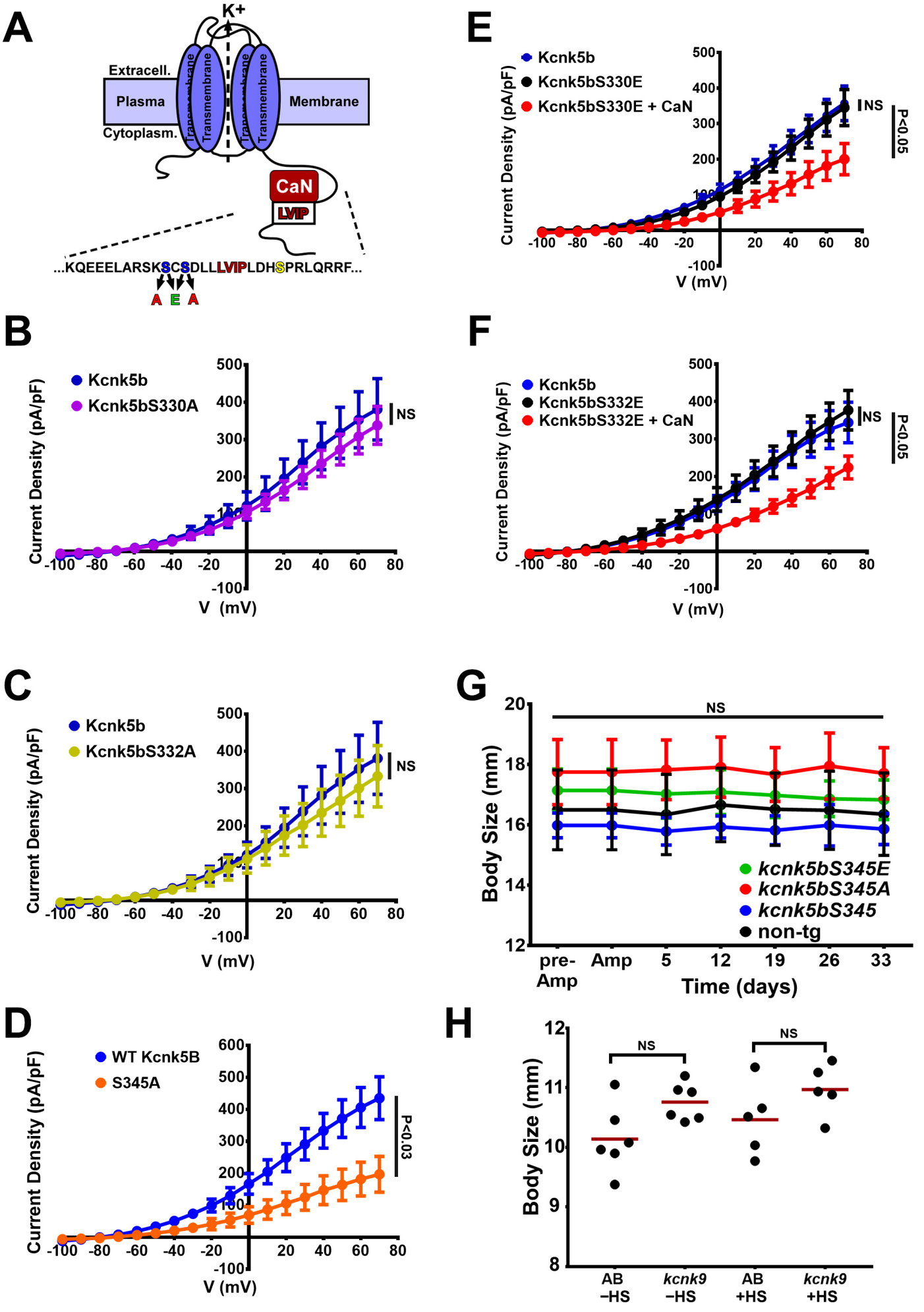

Yi et al., Fig. 6-Suppl. Fig. 1

Scaling Information

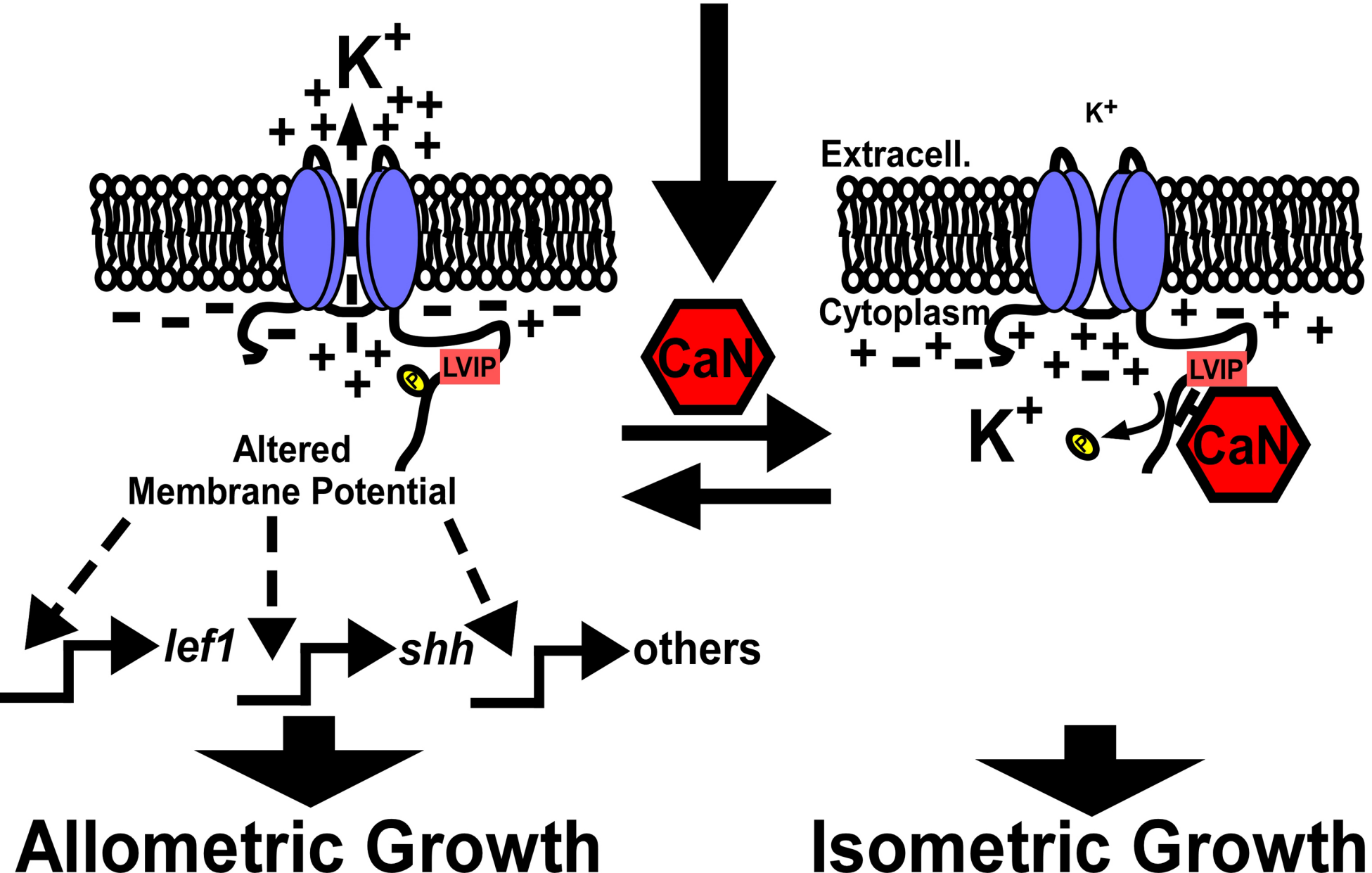

Table 1 qRT-PCR primer sequences for zebrafish genes

F-lef1	AATGATCCCGTTCAAAGACG
R-lef1	CGCTAAGTCTCCCTCCTCCT
F-shha	CCACTACGAGGGAAGAGCTG
R-shha	GAGCAATGAATGTGGGCTTT
F-aldh1a2	AACCACTGAACACGGACCTC
R-aldh1a2	CTCCAGTTTGGCTCCTTCAG
F-pea3	AGAAGAACCGTCCAGCCATGA
R-pea3	AACATAACGCTCACCAGCCAC
F-msxb	ACACTTTGTCGAGCGTTTCGG
R-msxb	TCTTGTGCTTGCGTAAGGTGC
F-ptch1	GGGCAGCTAATCTGGAGACGG
R-ptch1	GCGCCTCTACGGTCAAAATG
F-ptch2	TGCCACGCCGCTTTTGCTTT
R-ptch2	GTTTCAATGGCAGCGACCCG
F-bmp2a	GCAGAGCCAACACTATCAGGAG
R-bmp2a	CCACTTTAATACAGCAGGAGTTACG
F-axin2	GGACACTTCAAGGAACAACTAC
R-axin2	CCTCATACATTGGCAGAACTG
F-cmyc	TAACAGCTCCAGCAGCAGTG
R-cmyc	GCTTCAAAACTAGGGGACTG
F-cyclinD1	GCCAAACTGCCTATACATCAG
R-cyclinD1	TGTCGGTGCTTTTCAGGTAC
F-β-actin2	GCAGAAGGAGATCACATCCCTGGC
R-β-actin2	CATTGCCGTCACCTTCACCGTTC
F-kcnk5b	ATCACTCTCCTCGTCTGCAACG
R-kcnk5b	GAGTCCCATGCACAACGTGCAG
F-GFP	AAGGGCATCGACTTCAAGG
R-GFP	TGCTTGTCGGCCATGATATAG

Table 2 qRT-PCR primers for human genes

F-lef1	CTACCCATCCTCACTGTCAGTC
R-lef1	GGATGTTCCTGTTTGACCTGAGG
F-shh	CCGAGCGATTTAAGGAACTCACC
R-shh	AGCGTTCAACTTGTCCTTACACC
F-aldh1a2	GAGTAACTCTGGAACTTGGAGGC
R-aldh1a2	ATGGACTCCTCCACGAAGATGC
F-pea3	AGGAACAGACGGACTTCGCCTA
R-pea3	CTGGGAATGGTCGCAGAGGTTT
F-msx1	GACTCCTCAAGCTGCCAGAAGA
R-msx1	ACGGTTCGTCTTGTGTTTGCGG
F-GAPDH	GTCTCCTCTGACTTCAACAGCG
R-GAPDH	ACCACCCTGTTGCTGTAGCCAA

Table 3: primer sequences for qPCR genotyping

F-mCherry	GGCCATCATCAAGGAGTTCATGC
R-mCherry	GAGGGGAAGTTGGTGCCGC
F-β-actin	GAGCTGCAGTCTAAGCTTTGACC
R-β-actin	CATTGCCGTCACCTTCACCGTTC

Table 4: primer sequences for mouse qPCR

F-lef1	ACTGTCAGGCGACACTTCCATG
R-lef1	GTGCTCCTGTTTGACCTGAGGT
F-shh	GGATGAGGAAAACACGGGAGCA
R-shh	TCATCCCAGCCCTCGGTCACT
F-aldh1a2	CACAAGACACGAGCCCATTGGA
R-aldh1a2	GGTTTGATGACCACGGTGTTACC
F-pea3	CACAGACTTCGCCTACGACTCA
R-pea3	GCAGACATCATCTGGGAATGGTC

F-msx1	AGGACTCCTCAAGCTGCCAGAA
R-msx1	CGGTTGGTCTTGTGCTTGCGTA
F-GAPDH	CATCACTGCCACCCAGAAGACTG
R-GAPDH	ATGCCAGTGAGCTTCCCGTTCAG